Global and Planetary Change 242 (2024) 104589

Contents lists available at ScienceDirect

Global and Planetary Change

journal homepage: www.elsevier.com/locate/gloplacha

Mercury enrichments as a paleo-volcanism proxy: Sedimentary bias and a critical analysis across the end-Triassic

Xia Hua [a,b], David B. Kemp [a,*], Jun Shen [c], Runsheng Yin [d], Xin Jin [e], Chunju Huang [a]

[a] State Key Laboratory for Biogeology and Environmental Geology and Hubei Key Laboratory of Critical Zone Evolution, School of Earth Sciences, China University of Geosciences (Wuhan), Wuhan 430074, PR China
[b] Institute of Ocean Research, Peking University, Beijing 100871, China
[c] State Key Laboratory for Biogeology and Environmental Geology, China University of Geosciences (Wuhan), Wuhan 430074, PR China
[d] State Key Laboratory of Ore Deposit Geochemistry, Institute of Geochemistry, Chinese Academy of Sciences, Guiyang, Guizhou 550081, PR China
[e] State Key Laboratory of Oil and Gas Reservoir Geology and Exploitation, Chengdu University of Technology, Chengdu, Sichuan 610059, PR China

ARTICLE INFO

Editor: Dr. Maoyan Zhu

Keywords:
Hg anomaly
Paleo-volcanism
Late Triassic
Sedimentary facies

ABSTRACT

Mercury (Hg) anomalies in sedimentary rocks have been increasingly used in paleoclimatology studies for tracing volcanic signals, as Hg emissions from volcanic activity can cause contemporaneous sedimentary Hg enrichment. However, non-volcanic sedimentary controls on Hg have clear potential to mask these signals. These factors include host phase variability linked to environmentally controlled sourcing and settling changes, and/or variable preservation conditions associated with weathering, oxidation and diagenesis. Such factors can limit the efficacy of Hg as a paleo-volcanism proxy. In this study, sedimentary effects on Hg concentration within a complex depositional system in southwest England (St. Audrie's Bay) across the end-Triassic have been analyzed, together with published data from coeval end-Triassic sections globally – an interval of time coeval with the Central Atlantic Magmatic Province (CAMP). Our statistical analysis of Hg and associated geochemical data highlights significant fluctuations in sedimentary Hg due to relative supply differences in Hg and host phases, as well as the changing types and preservation conditions of host phases. End-Triassic sections globally show a consistent undersupply of Hg relative to organic matter across the end-Triassic mass extinction (ETME). To better assess the magnitude and significance of possible Hg enrichments in sedimentary rocks, we present a statistical method for quantifying Hg anomalies to robustly distinguish Hg variations linked to host phase/depositional changes from paleo-volcanism. Our method supports the existence of transient but asynchronous Hg anomalies linked to volcanism from the CAMP across the end-Triassic in most global sections, albeit not in the St. Audrie's Bay section.

1. Introduction

The measurement of sedimentary mercury (Hg) concentrations has become widely used for tracing large-scale paleo-volcanism, such as that associated with large igneous province (LIP) emplacement. Hg anomalies in ancient sedimentary rocks have been used to understand the causal links between LIPs and biological/environmental perturbations in geological history (Sanei et al., 2012; Grasby et al., 2019; Shen et al., 2019a, 2020, 2023). Hg in the natural environment is sourced primarily from magmatic Hg outgassing (Selin, 2009). Hg released from volcanism is mostly in the gaseous Hg^0 phase, which has an atmospheric residence time of 0.5 to 2 years, allowing its global transport and deposition on geologically short timescales (e.g., Selin, 2009). Gaseous Hg^0 is removed from the atmosphere via (i) oxidation to water-soluble Hg^{2+}, which is readily deposited to the ocean via precipitation; and (ii) fixation of Hg^0 by vegetation, which is then transferred into terrestrial soil via litterfall (dry deposition). Organic matter, sulfides, and clay are common hosts of Hg in sediments (Ravichandran, 2004). To recognize volcanic Hg inputs into sediments, it has become standard practice to normalize Hg concentrations to total organic carbon (TOC) concentrations, since organic matter is commonly deemed the major host of Hg (Grasby et al., 2019; Shen et al., 2020). Recent work, however, has drawn attention to the importance of identifying the exact host phases prior to normalization, largely based on correlation analysis between Hg and other potential host phases (e.g., Sanei et al., 2012; Shen et al., 2019b, 2020; Kovács et al., 2024; Zhu et al., 2024). Syn-depositional processes such as

* Corresponding author.
E-mail address: davidkemp@cug.edu.cn (D.B. Kemp).

https://doi.org/10.1016/j.gloplacha.2024.104589
Received 6 May 2024; Received in revised form 7 August 2024; Accepted 15 September 2024
Available online 16 September 2024

oxidation, organic matter degradation and weathering can also affect the preservation of Hg signals in sediments and rocks (Charbonnier et al., 2020; Park et al., 2022). Thus, compiled evidence of host phase variations and syn-depositional factors is needed to fully understand the influences of sedimentary processes and preservation state on Hg before using Hg as a volcanic proxy.

The end-Triassic mass extinction (ETME) was a key geological time interval that has been widely studied using the Hg paleo-volcanism proxy. This mass extinction, and associated paleoenvironmental changes, are thought to have been causally related to pulsed large-scale volcanism from the Central Atlantic Magmatic Province (CAMP) associated with Central Atlantic rifting (e.g., Blackburn et al., 2013; Davies et al., 2017; Lindström et al., 2021, and references therein). Multiple negative carbon isotope excursions (NCIEs) across the ETME have been attributed to large-scale ^{12}C-enriched carbon release from this LIP and/or other surficial reservoirs (e.g., Hesselbo et al., 2002; Ruhl et al., 2011; Davies et al., 2017). Hg/TOC anomalies have been reported during the ETME interval in widely distributed marine and terrestrial environments, including in the NW European epicontinental sea, northern/eastern Tethys margin and eastern Panthalassa margin (Thibodeau et al., 2016; Percival et al., 2017; Lindström et al., 2019, 2021; Shen et al., 2022a, 2022b; Bos et al., 2024). These Hg enrichments are readily attributable to CAMP volcanism. Nonetheless, a recent study at one of the most well-studied Triassic-Jurassic sections in St Audrie's Bay, UK (near the northern flank of CAMP), showed that anomalously high Hg/TOC across the ETME here was attributable to very low TOC abundance, and that in fact organic matter was unlikely to have been the major host phase of Hg (Hua et al., 2023). This observation also raises questions regarding the magnitude of Hg supply during the ETME, and whether Hg supply truly exceeded the maximum normal drawdown capacity of host phases (e.g., Grasby et al., 2019). Importantly, sedimentary Hg anomalies are seldom quantitatively defined and hence lack statistical appraisal, making it difficult to compare data both stratigraphically and between different study sites. In addition, most ETME global sections lack investigation of possible alternative Hg host phases, or the potential depositional controls on Hg concentration.

A marked and abrupt negative carbon isotope excursion (NCIE) across the ETME (the so-called 'initial NCIE' in Hesselbo et al., 2002) is coeval with elevated Hg/TOC in many sites, and this NCIE has previously been linked to emission of ^{12}C-enriched carbon from volcanism (Hesselbo et al., 2002; Korte et al., 2009; Ruhl and Kürschner, 2011; Ruhl et al., 2011; Lindström et al., 2021). However, work by Fox et al. (2020) has argued that in UK sections at least, this 'initial NCIE' was not linked to volcanism but resulted instead from regional organic matter source changes related to sea-level change. Variations in relative sea level throughout the Late Triassic have been established (Hallam, 2001; Hesselbo et al., 2004). These variations are evident from the formation of hiatuses in the European epicontinental area (e.g., Lindström et al., 2017), as well as in the depositional environment at St. Audrie's Bay, which transitioned from terrestrial to marine from the Late Triassic to the Early Jurassic (Hesselbo et al., 2004). Thus, the purported lack of anomalously high Hg enrichment across the ETME at St. Audrie's Bay (Hua et al., 2023), coupled with the marked environmental changes that occurred in this section, make it an excellent locality to re-examine the sedimentary controls on Hg and evaluate the efficacy of Hg as a volcanic proxy by comparison to other sites globally.

In this study, we present new inorganic and organic geochemistry data from the St. Audrie's Bay section, together with a compilation of published data from other ETME sections globally. Our goals are to: 1) identify sedimentary and *syn*-depositional controls on Hg concentration at St Audrie's Bay and other sections, 2) establish a new statistical approach for robustly quantifying Hg enrichment in sedimentary rocks, 3) critically evaluate possible paleo-volcanism signals across the end-Triassic globally.

2. Geological setting of the studied sections

2.1. St Audrie's Bay

St Audrie's Bay (51.182°N, 3.286°W) is located in Somerset, southwest England and contains a ~ 48 m outcrop of strata spanning the Late Triassic (Norian-Rhaetian) to Early Jurassic (Hettangian) (Fig. 1). The lithostratigraphy and depositional environments of the section have been studied in detail by previous workers, and are summarized below.

The Blue Anchor Formation (Norian to Rhaetian) consists of the Rydon Member and overlying Williton Member. The Rydon Member comprises ~28 m of alternating green-grey mudstones, grey siltstones and grey-yellowish dolostones (Warrington and Whittaker, 1984). Also present are evaporitic features (collapse breccias, halite pseudomorphs) and evidence of extreme shallowing and ephemeral subaerial exposure (ripples and desiccation cracks) (Mayall, 1981; Warrington and Whittaker, 1984). Dark mudstones occur in places (Thomas et al., 1993), and total organic matter content (TOC) reaches up to 3 wt% (Hua et al., 2023). The lithostratigraphy and absence of marine fossils suggest a largely non-marine, possibly sabkha-like, environment (Warrington and Whittaker, 1984), with ephemeral marine incursion indicated by previous organic geochemical work (Thomas et al., 1993). The overlying Williton Member rests unconformably on the Rydon Member, and consists of ~2 m of mainly green-grey silty mudstones with marine trace fossils and bivalves, interpreted as shallow marine (Mayall, 1981; Hesselbo et al., 2004).

Unconformably overlying the Williton Member is the Westbury Formation, which is characterized by ~9 m of grey to dark grey mudstones and silty mudstones with localized carbonate concretions. Near the base, 'bone' beds occur (Macquaker, 1987), which consist mainly of bivalves and vertebrate debris of fish and reptiles (Ivimey-Cook et al., 1999). The Westbury Formation was likely deposited in a relatively small, restricted marine basin largely separated from the circulatory systems of the Tethys Ocean (Macquaker, 1987). Marine fossils (such as brachiopods, sponges, codononts, ammonoids, bryozoans and corals) are relatively rare (Suan et al., 2012; Wignall and Atkinson, 2020). Conditions were largely quiescent, though with occasional transgression and storm influence (Macquaker, 1987; Wignall, 2001; Suan et al., 2012; He et al., 2022).

Above the Westbury Formation is the ~2 m thick Lilstock Formation. This can be divided into the Cotham and Langport members. The lower part of the Cotham Member is characterized by thinly interbedded siltstone and fine-grained sandstone with common waveripples (Hesselbo et al., 2004). The transition from the Westbury Formation represents a shallowing of the depositional environment from shallow shelf to peritidal (Wignall and Bond, 2008). The upper part of the Cotham Member contains large dessication cracks, and consists of interbedded mudstone and siltstone with wave-ripples and ooids (Hesselbo et al., 2004). It is hypothesized to be deposited in a coastal environment with rising relative sea level (Hesselbo et al., 2004; Wignall and Bond, 2008). The ~1 m thick Langport Member consists of limestone and calcareous mudstone, and is interpreted to have been deposited in an entirely submarine environment, with sediment starvation occurring as a consequence of sea level rise (Swift, 1999; Hesselbo et al., 2004).

The overlying Blue Lias Formation consists of interbedded dark grey (sometimes laminated) shales, marls and limestones. The fully marine fauna has a notable change upwards from the basal Blue Lias Formation. Bivalves dominate the lowermost ~5 m of the formation (the so-called Pre-*planorbis* Beds), while upwards the assemblages change to become ammonite-dominated (Hesselbo et al., 2004). Laminated facies and variations in burrowing intensity, together with pyrite framboid abundance and Fe speciation data, indicate euxinic conditions followed by a transition towards a more fluctuating redox state between anoxic-ferruginous and euxinic conditions in a restricted fully marine setting (Wignall, 2001; He et al., 2022; Fox et al., 2020).

Although the Triassic-Jurassic succession at St. Audrie's Bay has

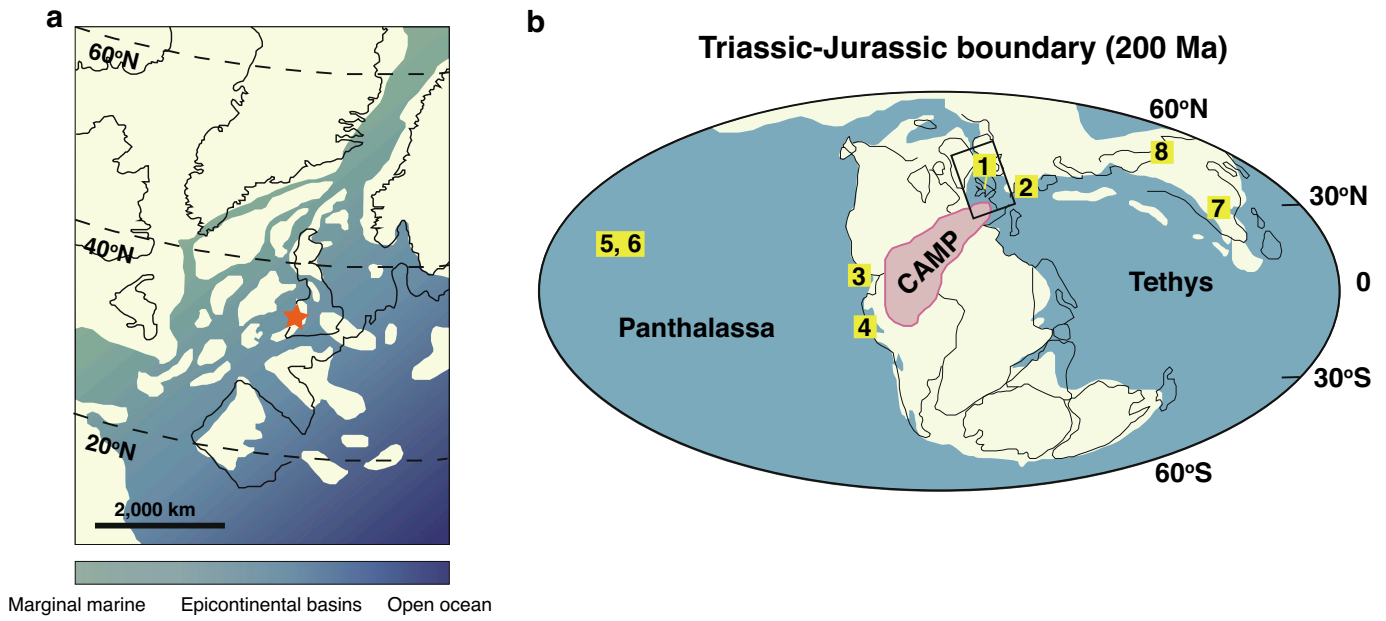

Fig. 1. Paleogeographic maps and and location of the studied sections. a, Paleogeographical map showing location of St Audrie's Bay (red star). b, Global paleogeographic reconstruction at the Triassic-Jurassic, with the location of the Central Atlantic Magmatic Province (CAMP) highlighted, as well as ETME sections discussed in the text: 1. St Audrie's Bay (this study), 2. Kuhjoch (Percival et al., 2017), 3. New York Canyon (Thibodeau et al., 2016), 4. Levanto (Yager et al., 2021), 5. Kurusu (Schoepfer et al., 2022), 6. Katsuyama (Shen et al., 2022b), 7. Qilixia (Shen et al., 2022a), 8. Haojiagou (Shen et al., 2022a). Figure is modified from He et al. (2022). (For interpretation of the references to colour in this figure legend, the reader is referred to the web version of this article.)

been well-studied, there is no consensus on the precise stratigraphic position of the ETME. The base of the ETME here was originally placed near the sharp 'initial' NCIE within the Lilstock Formation (Hesselbo et al., 2002; Warrington et al., 2008). Lindström et al. (2017, 2021) defined the ETME globally, and correlated the ETME base to an older NCIE (named the Marshi NCIE) in the Westbury Formation (35.85 m) (Fig. 2, see also Suan et al., 2012). The original initial NCIE was instead correlated to the younger Spelae NCIE by Lindström et al. (2017, 2021, 40.85 m), which elsewhere precedes the FO of *Psiloceras spelae* (TJB). In this study, we follow the global correlation and ETME definition of Lindström et al. (2017, 2021).

2.2. Data compilation of global ETME sections

Hg and associated compositional data are compiled from 7 published ETME sections deposited in varying depositional environments worldwide (Fig. 1). The studied sections are: the Kuhjoch section in Austria, the New York Canyon section in Nevada, USA, the Levanto section in Peru, the Kurusu section and Katsuyama sections in Japan, and the Haojiagou and Qilixia sections in China.

Carbon isotopes and biostratigraphical data from the compiled sections permit the delineation of the ETME and different carbon isotope events (i.e. Marshi NCIE and Spelae NCIE). The Kuhjoch section in Austria is the global stratotype section and point (GSSP) for the base of the Hettangian Stage (i.e. the Triassic-Jurassic boundary, Hillebrandt et al., 2013). It is characterized by limestone and marl, with a highly condensed layer of black shale at the onset of the marine extinction horizon (Hillebrandt et al., 2007, 2013). It was deposited in an open shallow marine setting in the northwestern Tethys Ocean (Hillebrandt et al., 2007, 2013; Bonis et al., 2009). The Hg and TOC data of Kuhjoch section are from Percival et al. (2017). The New York Canyon section in Nevada, USA is characterized by calcareous siltstone and silty limestone deposited on an open shallow shelf environment in the Panthalassa Ocean (Lucas et al., 2007). The Hg and TOC data of the New York Canyon section are from Thibodeau et al. (2016). The Levanto section in Peru is characterized by carbonate-rich mudstones with abundant intercalated ash beds, which are interpreted to have been deposited in an anoxic shallow marine environment on the eastern Panthalassic margin (Yager et al., 2017). The Hg and TOC data of the Levanto section are from Yager et al. (2021). The Kurusu and Katsuyama sections in

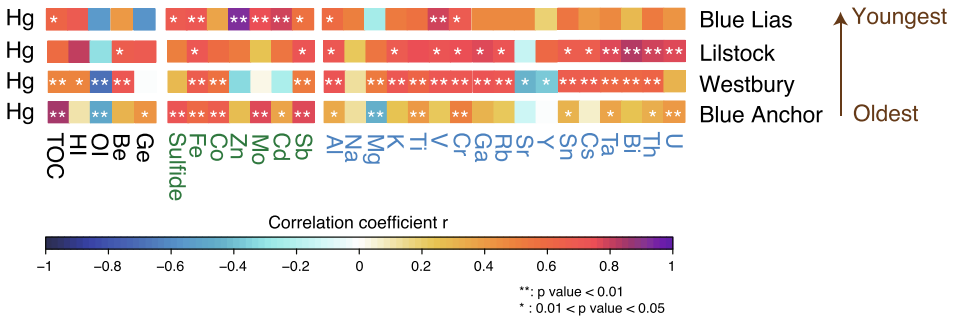

Fig. 2. Correlation heatmaps between Hg, major host phases and other whole-rock element abundances, split by formation. Significance levels (based on correlation coefficient *p* values) are also indicated. Elements are grouped based on their affinities with organic matter (black text), sulfides (green text) or clays/lithophile phases (blue text). See main text for details. The ETME interval is within the Westbury and Lilstock Formations. (For interpretation of the references to colour in this figure legend, the reader is referred to the web version of this article.)

Japan are characterized by thinly interbedded chert and shales deposited in a pelagic deep marine environment in central Panthalassa (Wignall et al., 2010; Ikeda and Tada, 2014; Ikeda et al., 2017). The Hg and associated compositional data of these two sections are from Schoepfer et al. (2022) and Shen et al. (2022b), respectively. The Haojiagou section in China is characterized by mudstone and siltstone with interbedded coal and black mudstone, deposited in a high-latitude lacustrine environment (Sha et al., 2011). The Qilixia section in China is characterized by sandstone, siltstone, mudstone, and coal seams with abundant plant fossils deposited in a low/middle latitude fluvial environment (Li et al., 2020). Hg and associated compositional data from both the Haojiagou and Qilixia sections are from Shen et al. (2022a).

3. Methods

3.1. Major and trace element analyses

100 samples were collected across a 49.1 m interval from the Blue Anchor Formation to the Blue Lias Formation, and is the same sample suite analyzed in Hua et al. (2023). Hg, S (sulfide) and Al abundance data on these samples were previously presented in Hua et al. (2023). Other elements, including major and trace elements, were measured on the samples using an Agilent-5110 ICP-OES or Agilent 7900 ICP-MS at ALS Chemex (Guangzhou) Co., Ltd. A four-acid digestion method of HNO_3–$HClO_4$–HF–HCl was conducted in three steps to dissolve most of the minerals. HNO_3 and $HClO_4$ were first used for pre-oxidation followed by HF addition to digest silicate and aluminate phases. The solution was then evaporated and HCl was added before measurements. Multiple replicate analyses of standards yielded typical analytical precisions of better than ±10 % (RSD).

Enrichment factors for element abundances were calculated as $X_{EF} = (X/Al)_{sample}/(X/Al)_{PAAS}$, where X is the element being quantified and PAAS refers to post-Archean Australian shale (data from Taylor and Mclennan, 1985). If X_{EF} is greater than 1, then element X is enriched relative to PAAS, otherwise it is depleted. In practice, a detectable enrichment corresponds to $X_{EF} > 3$ and a substantial enrichment to $X_{EF} > 10$ (following Algeo and Tribovillard, 2009).

3.2. Organic geochemical analysis

Organic matter pyrolysis of a subset of 75 powdered samples was conducted using a Rock Eval 6 instrument at the Guangzhou Institute of Geochemistry, Chinese Academy of Sciences, following the method described in Espitalié et al. (1985). The IFP 160000 standard was used for calibration. Hydrogen Index (HI, mg HC g^{-1} TOC), Oxygen Index (OI, mg CO_2 g^{-1} TOC) and T_{max} (°C) were determined.

3.3. Scanning electron microscopy

Polished blocks (3 cm × 2 cm) from the St Audrie's Bay section were made for in situ observation and element mapping (specifically of framboidal pyrite) using a FEI Quanta 200 scanning electron microscope (SEM) at the State Key Laboratory of Geological Processes and Mineral Resources, China University of Geosciences (Wuhan). The spatial resolution of the secondary electron image of SEM was better than 3.5 μm. In backscattered electron (BSE) images, framboidal crystal pyrite can be distinguished from pyrite microlites (i.e. formed during early lithification) by their shapes and structures. C, Al, S, Fe, Mo, and Hg were targeted for quantitative measurement using Energy Dispersive X-Ray Spectroscopy (EDS) element mapping.

4. Results

4.1. Correlations between Hg and other whole-rock element abundance at St Audrie's Bay

To assess the relationship between the Hg and other elements in the St. Audrie's Bay section, we employ correlation analysis. Whole-rock geochemical correlation heatmaps illustrate the variability in the associations between specific elements and Hg, which is useful to assess the changing affinity behavior of Hg across the section (Fig. 2). Hg within the Blue Anchor Formation shows significant and at least moderately strong correlations (i.e. $r > 0.6$, $p < 0.01$) with TOC, Sb, Mo, sulfide, Tl, Co, As, Ag, and Fe (Fig. 2). In the Westbury Formation, Hg correlates significantly and at least moderately strongly (i.e. $r > 0.6$, $p < 0.01$) with Al, Ga, In, Sc, K, Cr, Be, Rb, V, Ni, Cs, Li, Sn, Fe, Cu, Th, Ti, W, Ta, Bi and Nb (Fig. 2). In the Lilstock Formation, Hg correlates significantly and at least moderately strongly (i.e. $r > 0.6$, $p < 0.01$) with Sc, Cu, Nb, In, Ta, Bi, Th, and U (Fig. 2). In the Blue Lias Formation, Hg correlates significantly and at least moderately strongly with V, Fe, Ni, Zn, Mo, Cd, and Tl (Fig. 2).

4.2. Rock Eval pyrolysis at St Audrie's Bay

T_{max} values through the St. Audrie's Bay section are broadly stable, ranging from ~410 to 504 °C (mean = 424 °C). Two outlying values of 465 and 504 °C occur in the Blue Anchor Formation. Hydrogen index (HI) values range from 19 to 167 mg HC/g TOC in the Blue Anchor Formation. HI shows a relatively wider range of 69 to 515 mg HC/g TOC in the Westbury Formation, with a large increase coincident with the Marshi NCIE at ~35.85 m (Fig. 3). The Lilstock Formation shows relatively low HI values (averaging 59.2 mg HC/g TOC), followed by a significant increase up to 826 mg HC/g TOC at the top of the Blue Lias Formation (Fig. 3). Oxygen index (OI) in the Blue Anchor Formation ranges from 4 to 300 mg CO_2/g TOC (mean = 68.7 mg CO_2/g TOC), with widely fluctuating values (19 to 300 mg CO_2/g TOC) in the basal ~14 m. OI in the Westbury Formation ranges from 4 to 177 mg CO_2/g TOC (averaging 36.2 mg CO_2/g TOC). OI is relatively higher in the Lilstock Formation (averaging 260.6 mg CO_2/g TOC) and most of the Blue Lias Formation. However, towards the top of the Blue Lias Formation there is an abrupt decrease down to ~15 mg CO_2/g TOC (Fig. 3).

5. Discussion

5.1. Hg host phase transitions and syn-depositional controls on Hg concentration at St Audrie's Bay

Our analysis of the correlations between Hg and multiple elements and rock components is useful for distinguishing host phase variations through the St. Audrie's Bay succession, and how Hg behavior could be influenced by both changing environment and possible syn-depositional factors. Notably, whole-rock element abundance data offer an efficient way of assessing the overall composition of sedimentary rocks, potentially with greater precision than can be attained using XRD analysis of mineralogical composition (especially when minerals that may host Hg are present in low amounts, e.g., Zhu et al., 2024).

Minerals can been categorized based on their associations with certain elements (e.g., Kersten and Forstner, 1989; Ure and Davidson, 2002), particularly in coals (Querol et al., 1995; Vejahati et al., 2010), such as iron sulfides and their inclusion of Co, Ni, Cu, Zn, As, Mo, Cd, Sb, W, Tl and Pb (Gregory et al., 2015). Clay minerals and feldspars are associated with dominantly lithophile elements, i.e. Al, Na, Mg, K, Ti, V, Cr, Ni, Cu, Ga, Rb, Sr, Y, Sn, Cs, Ta, Pb, Bi, Th and U (Querol et al., 1995). Organic matter can be associated with elements such as Be, Ge, As, and W (Querol et al., 1995), owing mainly to complexation and sorption processes (e.g., Mostofa et al., 2013). Examing the variation in associations between specific elements and Hg could help to assess the

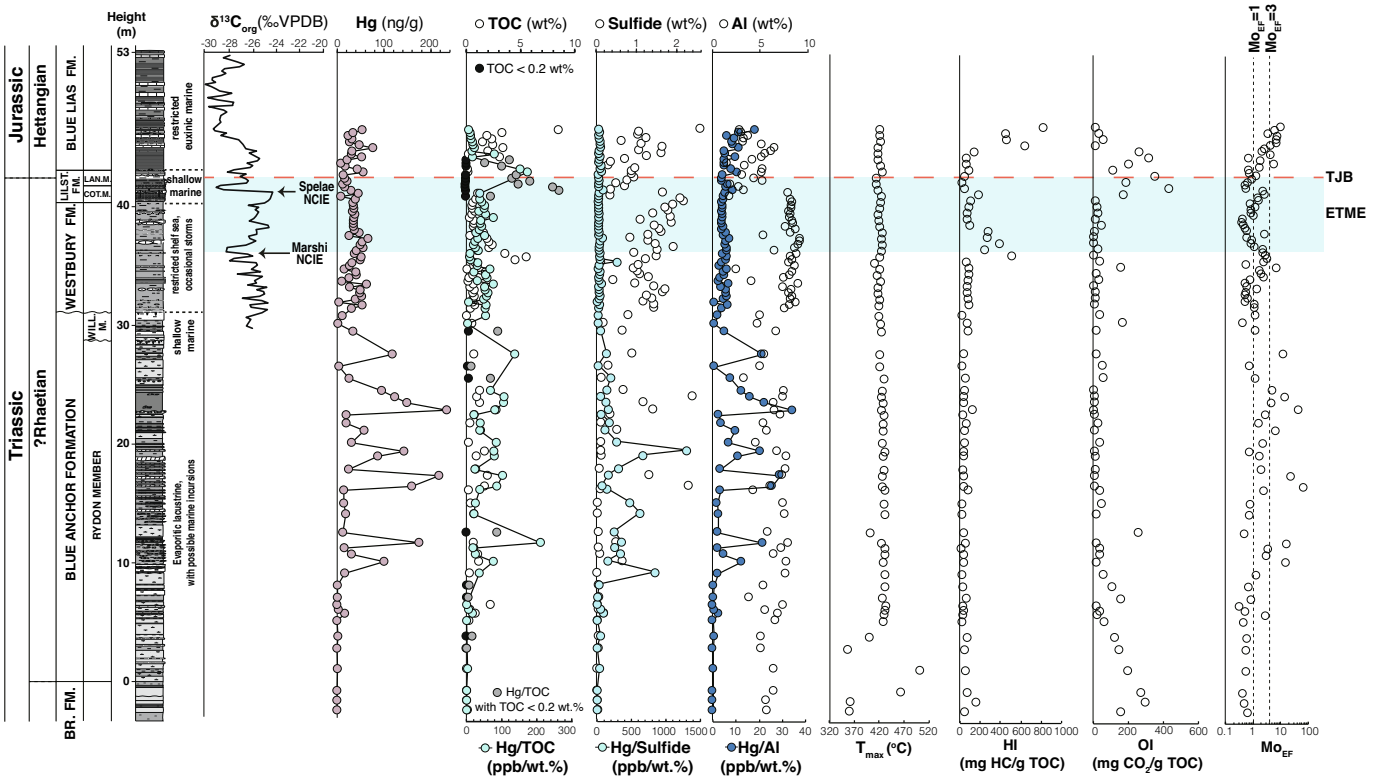

Fig. 3. Stratigraphic variations in Hg and other key geochemical data at St Audrie's Bay. Hg and major host phases (TOC, sulphide, Al – a proxy for clay) data are from Hua et al. (2023). Organic geochemistry data T_{max}, HI, OI and Mo enrichment factor (Mo_{EF}) are from this study. Sedimentary log is from Hua et al. (2023). Samples with TOC <0.2 wt% are indicated (see Section 5.2). CIE: carbon isotope excursion. The shaded ETME interval (end-Triassic mass extinction) and dashed line marking the TJB (Triassic Jurassic Boundary) are based on Lindström et al. (2021).

changing affinity behavior of Hg with different components stratigraphically (Fig. 2). Nevertheless, element behaviors can be complex during deposition from either atmospheric or fluvial pathways (i.e. sorting, leaching or adsorption process can all result in changes in element preservation, Calvert and Pedersen, 2007).

In the Blue Anchor Formation, elements that have strong positive correlations ($r > 0.6, p < 0.01$) with Hg are typically associated in sulfide minerals (As, Co, Mo, Sb and Tl, consistent with the Hg – host correlation analysis in Hua et al., 2023, Fig. 2), but Hg also correlates very clearly with TOC. The Rydon Member (in the lowest 28 m of the Blue Anchor Formation) is interpreted to have formed on the margins of an evaporitic lake, akin to a modern sabkha environment, with probably only ephemeral marine connection (Mayall, 1981; Thomas et al., 1993; Hesselbo et al., 2004). Brines percolating during deposition of the Blue Anchor Formation were likely of mixed marine and continental origin (Taylor, 1983; see also Thomas et al., 1993). Under high salinity conditions such as those that may have characterized the Blue Anchor Formation depositional environment, the oxidation of elemental Hg to Hg^{2+} can be stimulated by chloride ions (Yamamoto, 1996), which may be beneficial for promoting Hg drawdown and preservation. The presence of reducing conditions in hypersaline basins is facilitated by restricted circulation caused by salinity (density) contrasts. Previous work has suggested that Mo/Al enrichment is favored in modern anoxic hypersaline basins and is closely correlated with TOC content (e.g., Oliveri et al., 2013). At St. Audrie's Bay, Mo_{EF} peaks within the Blue Anchor Formation coincide with Hg and sulfide peaks (Fig. 3). Intermittent reducing conditions are likely to have occurred in the Blue Anchor Formation (Thomas et al., 1993), which could have enhanced the adsorption of Hg into sediment via sulfide production. The presence of dissolved sulfide could convert molybdate (MoO_4^{2-}) to particle-reactive thiomolybdates ($MoO_xS_{4-x}^{2-}$), causing further Mo sequestration by organic matter and sulfide minerals (Erickson and Helz, 2000). Enhanced organic matter preservation, formation of HgS and uptake of Hg by iron sulfides (Bower et al., 2008; Shen et al., 2019b, 2020) under occasionally reduced conditions could further explain the covariation patterns between Hg–TOC and Hg–sulfide.

Hg in both the Westbury and Lilstock Formations correlates most strongly with elements that are mostly hosted in clay minerals (notably Mg, K, Ti, V, Cr, Ga, Rb, Sn, Cs, Th in the Westbury Formation, and Ta, Bi, Th and U in the Lilstock Formation, Fig. 2). This supports the findings of Hua et a. (2023) that the major Hg host phase in both the Westbury and Lilstock Formations was clay, including across the ETME interval between 35.85 and 40.85 m (Fig. 3).

Clays have previously been found to be a host phase of Hg in both terrestrial and marine sediments (e.g., Shen et al., 2019c; Jin et al., 2022). Clay minerals can adsorb Hg^{2+} due to their high surface area and surface charges, and/or adsorb sparingly soluble $Hg(OH)_2$ in organic-lean sediments (Farrah and Pickering, 1978; Uddin, 2017). Although Hg adsorption capacity of clay might be less stable than organic matter and sulfide due to the weaker intermolecular forces between clay and Hg ions (Uddin, 2017), the adsorption capacity of different clay minerals varies (Farrah and Pickering, 1978; Kongchum et al., 2011). Mayall (1981) showed that the abundance of mixed-layer illite-smectite significantly increased (whilst illite decreased) from the Blue Anchor Formation into the Westbury Formation. This is coincident with an environmental transition from sabkha to shallow marine. Kongchum et al. (2011) showed smectite correlates well with Hg in modern sediments, probably because the specific surface area and cation exchange capacity of smectite are considerably larger than for other clay types (e.g., Uddin, 2017). The relative increase in smectite-bearing clay in the Westbury Formation relative to the Blue Anchor Formation may thus account for the Hg host phase transition from organic matter/sulfides to clays.

In the Blue Lias Formation, elements that correlate significantly ($r >$

0.6, $p < 0.01$) with Hg are typically those hosted in sulfide (Fe, Zn, Mo, Cd) (Fig. 2). EDS element mapping of a sample in the Blue Lias Formation (sample W54, 44.35 m) shows that Hg is hosted mainly in pyrite (both framboids and microlites, Fig. 4). In samples below this, EDS evidence of Hg enrichment in inferred hosts (i.e. organic matter and clays) was not clearly observed, likely owing to the very diffuse nature of these host phases in the rock matrix and the limited capability for relatively low concentrations of Hg to be mapped using EDS.

Redox conditions fluctuated between anoxic and oxic during deposition of the Lilstock Formation, but were predominantly euxinic during deposition of the Blue Lias Formation (Fox et al., 2020; He et al., 2022). This could account for the observed transition from clay to sulfide hosting at this time, because oxygen-depleted conditions favour the formation of Hg–sulfide complexes (Ravichandran, 2004). The formation of pyrite framboids in the water column or at the sediment-water interface under euxinic conditions would allow direct uptake of Hg from seawater. Hg in halogen complexes could also replace Fe in Fe-sulfide to form Hg mono- and bi-sulfide (Morse and Luther III, 1999). These processes could all simultaneously result in Hg enrichment in sulfides during deoxygenation.

The relative steepness of the Hg–host (i.e. TOC and sulfide) correlation slopes compared to other intervals is a key characteristic of the Blue Anchor Formation (Fig. 5). This means that there is relatively more variation in Hg content with changing host phase abundance compared to the other studied intervals, and that for a given concentration of sulfide or TOC, there is relatively more Hg in the Blue Anchor Formation compared to the other formations. This could, at least in part, explain the large fluctuations in Hg/TOC and Hg/sulfide values in the Blue Anchor Formation (Fig. 3; Hua et al., 2023). Sanei et al. (2014) suggested that steeper slopes in modern Hg–host correlation plots would arise if the Hg has a proximal source, which leads to a "vulnerable" aquatic system where Hg input exceeds the supply and/or the hosting efficiency of host phase (i.e. SH^- groups in the organic matter). Hua et al. (2023) inferred the likely predominance of terrestrial Hg in the Blue Anchor formation, supporting this interpretation of a proximal terrestrial Hg source. This is also consistent with other studies (both modern and geological), which suggested that locations closer to land would have relatively higher Hg abundance owing to terrestrial Hg delivery from rivers (i.e. Yin et al., 2015; Grasby et al., 2017; Them II et al., 2019).

In spite of two outlying T_{max} values (465 and 504 °C) in the Blue Anchor Formation, T_{max} values across the section as a whole are below 435 °C (Fig. 3), indicating a predominance of relatively immature and well-preserved organic matter with little post-depositional diagenetic alteration (Van Krevelen, 1981). Variations in organic matter sources can ostensibly be identified for each formation by the HI and OI data (Fig. 6). Van Krevelen diagrams show that the Blue Anchor formation is dominated by a mix of terrestrially derived Type III (higher plants) and IV (reworked/oxidized) organic matter.

It is particularly noteworthy that across the Blue Anchor Formation, samples with relatively high OI are commonly associated with lower Hg (and TOC) concentrations. Indeed, there is a non-linear inverse relationship between Hg and OI in the Blue Anchor Formation, which contrasts with the other formations (Fig. S1). In addition, Hg is absent in the samples with unusually high T_{max} (465 and 504 °C) (Fig. 3). High OI and low TOC samples reflect Type IV organic matter, and are likely to be reworked or oxidized, perhaps due to ephemeral subaerial exposure during deposition. This could lead to organic matter loss and the loss of volatile Hg. A similar loss of Hg linked to organic matter degradation during weathering has been noted by Charbonnier et al. (2020). Exposure to air during deposition could destroy the structure of the Hg-organic complex due to oxidation. Intermittant Hg loss via this process due to ephemeral subaerial exposure of the Blue Anchor Formation sediments could amplify Hg and Hg/TOC variability, thus accounting at least in part for the marked variability in Hg observed (0–233 ng/g).

In contrast to the steep Hg–TOC and Hg–sulfide correlation slopes observed in the Blue Anchor Formation, the shallow correlation slopes of Hg–host pairs across Westbury Formation to Blue Lias Formation (emcompassing the ETME interval) indicates an oversupply of host phases relative to Hg input (Fig. 5). This implies relatively low Hg supply

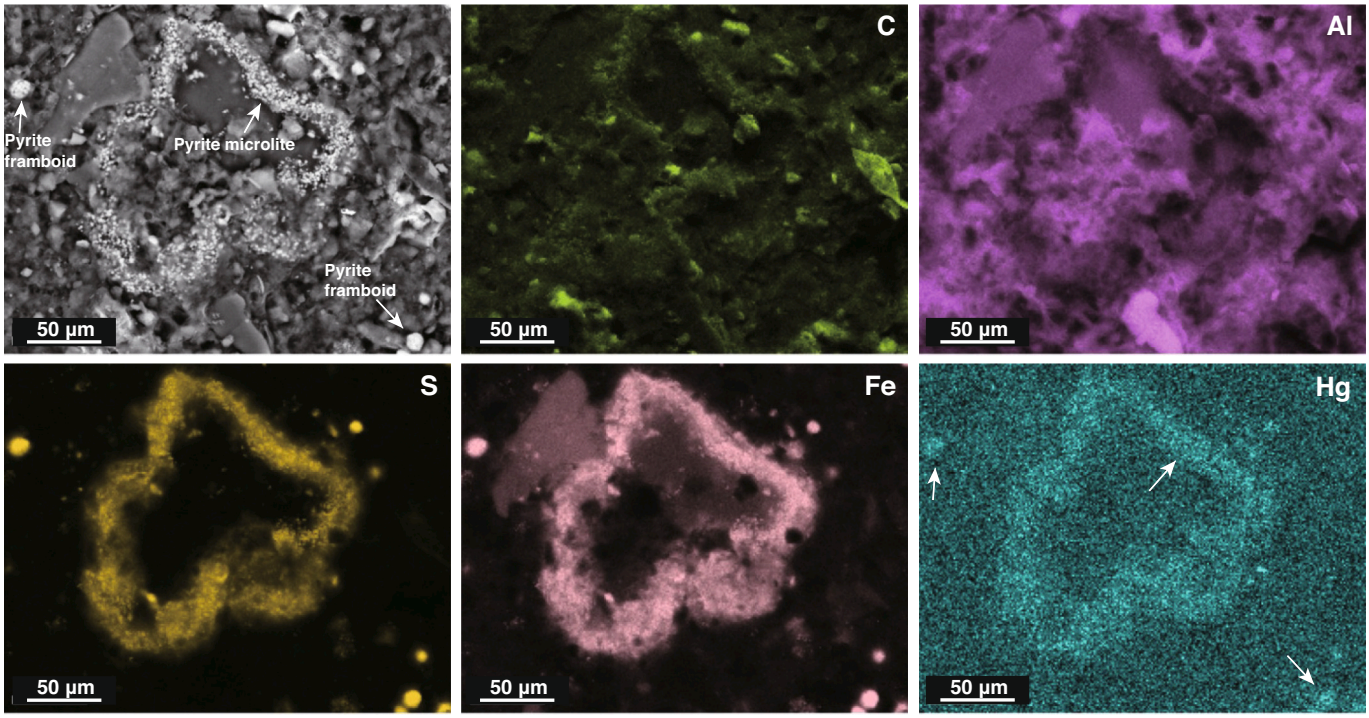

Fig. 4. SEM and EDS-derived element maps of sample W54 (44.35 m height in the Blue Lias Formation). Arrows point to framboidal pyrites and microlite pyrites. Note the elevated abundance of Hg in both the framboidal pyrites and microlite particles (brighter areas in image). See main text for details. (For interpretation of the references to colour in this figure legend, the reader is referred to the web version of this article.)

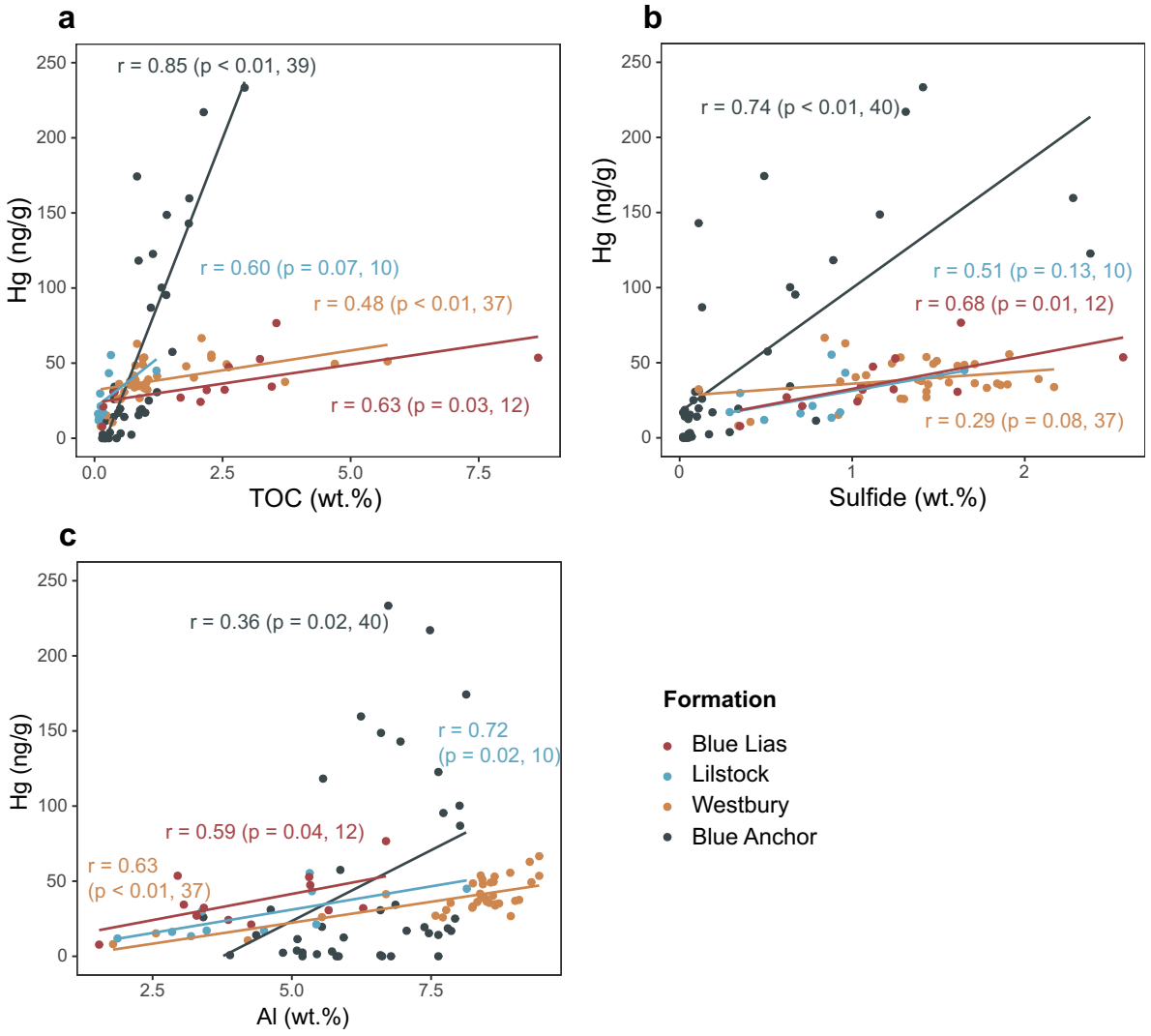

Fig. 5. Cross-plots of Hg and major Hg host phases (TOC, sulfide, Al) across individual formations at St. Audrie's Bay. a, Hg–TOC, b, Hg–sulfide, and c, Hg—Al (a proxy for clay content). Note the steeper slopes for the Blue Anchor Formation compared to the other formations. (For interpretation of the references to colour in this figure legend, the reader is referred to the web version of this article.)

and efficient scavenging and fixing of available Hg across ETME (Fig. 5). Hg and TOC content both show decreasing abundance with higher OI/lower HI across Westbury Formation to Blue Lias Formation (Fig. 6), although the correlations between Hg and OI are insignificant in Lilstock to Blue Lias Formations (Fig. S1), leaving the influence of changing organic matter types and *syn*-depositional oxidation on variations in Hg concentration within these formations uncertain.

5.2. *Limited global Hg loading compared to organic matter supply across the ETME*

As discussed in Section 5.1, St Audrie's Bay exhibits lower Hg loading across the ETME compared to the background interval (i.e. Blue Anchor Formation), in spite of the fact that CAMP volcanism was active across the ETME and generally considered to have been a significant source of exogenic Hg (Lindström et al., 2021 and references therein). To investigate this further, we compiled Hg and host phases data (mainly TOC data, see discussion below) from various ETME sections worldwide to examine the relative supply characteristics of Hg across the ETME on a global scale.

In most Hg studies across the ETME, routine analysis and identification of potential Hg host phases other than organic matter are lacking, with Al and sulfide data in particular rarely collected (i.e. Thibodeau et al., 2016; Percival et al., 2017; Yager et al., 2021). Other work has, however, established datasets that have determined the Hg host phases based on correlation analysis, such as at the Katsuyama section (Japan), where a dominant clay host was inferred from Th data (Shen et al., 2022b), and at the Kurusu section (Japan), where a host of non-acid volatile sulfur was inferred (Schoepfer et al., 2022). In the Qilixia and Haojiagou sections in China (Shen et al., 2022a), the host phase was determined to be organic matter. Nevertheless, organic matter is at least a contributary host phase of Hg under most circumstances, though its binding efficiency can be variable depending on the supply of other hosts such as clays and sulfides (Shen et al., 2020).

Here, correlations between available Hg and TOC data from St Audrie's Bay (this study), Levanto (Yager et al., 2021), New York Canyon (Thibodeau et al., 2016), Kuhjoch (Percival et al., 2017), Qilixia and Haojiagou (Shen et al., 2022a) are investigated in detail to assess Hg fluxes relative to organic matter host phase abundance changes. Following Grasby et al. (2019), samples with TOC < 0.2 wt% are excluded from the analysis. This is because such low TOC abundance is often close to the analytical precision of TOC measurements, and when TOC is very low even minor changes caused by analytical errors lead to large and inaccurate changes in Hg/TOC (Grasby et al., 2019). Data from

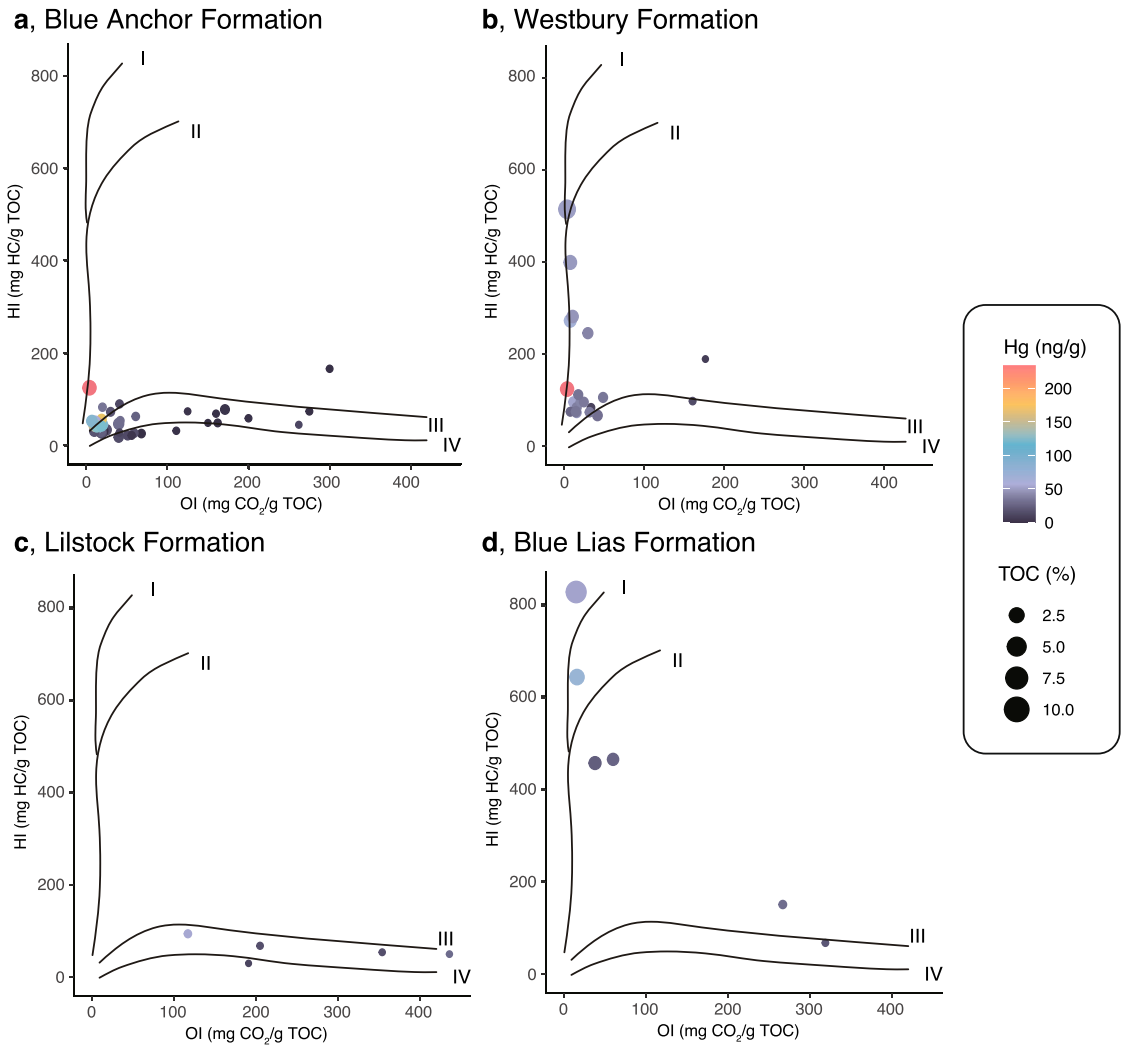

Fig. 6. van Krevelen diagrams for the pyrolysis data across individual formations at St. Audrie's Bay (Van Krevelen, 1981). Colors and sizes of the datapoints show the Hg concentrations and TOC abundances, respectively. Kerogens can be classified as Type I and II (of algal and marine-derived origin), and Type III and IV (likely from terrestrial higher plants with oxidized/reworked organic matter) (Van Krevelen, 1981; Espitalié et al., 1985).

before and after the ETME intervals of each section are assumed to represent background values without significant input of Hg from exogenic (i.e. volcanic) sources. As such, these data are separated from the data within the ETME interval for each section. The relationships between Hg concentrations and TOC in the background samples was examined for Hg–organic matter binding efficiency variation using linear regression (i.e. following Sanei et al., 2014; Fig. 7; see Fig. S2 for separate Hg – TOC crossplots for each site), with correlation coefficients also shown in Table 1. The results show that despite the significant positive correlations between Hg and TOC in part of the background interval at St Audrie's Bay (i.e. Blue Anchor Formation) and at Qilixia, the correlations in the shallow marine sections of Levanto, New York Canyon and Kuhjoch, and terrestrial Haojiagou section are insignificant. In part, this may relate to the low data quantity in some of these sections (Table 1), but it also suggests that organic matter is not the dominant Hg host at these localities (Fig. 7; Table 1; Fig. S2). Notably, the positive regression slope of the Blue Anchor Formation is the steepest of any dataset (Table 1; Fig. S2).

Within the ETME interval, weak and shallow correlations exist at most sites (Fig. 7; Table 1; Fig. S2), and the data plot below the maximum normal organic matter drawdown threshold (Fig. 7). This threshold was defined as a power law ($Hg = 150\ TOC^{0.83}$) by Grasby et al. (2019) and describes the maximum capacity of Hg sorption by organic matter, based on a data compilation of Hg and TOC data through the Phanerozoic.

Taken together, the end-Triassic data we have compiled within the ETME interval at the various sites suggest that Hg loading across the ETME was likely relatively limited, in clear contrast to Hg records spanning the end-Permian mass extinction for instance, which was coeval with Siberian Trap emplacement (Grasby et al., 2019; Fig. 7). These observations potentially call into question whether Hg was genuinely enriched and sourced exogenically (i.e. from CAMP volcanism) across the ETME. We thus investigate this below in the Section 5.3.

5.3. *Hg anomaly quantification using externally studentized residuals*

The Hg – TOC correlations from global ETME sections shown in Fig. 7 suggest that Hg input was largely undersupplied relative to organic matter. Nevertheless, elevated Hg/host ratios have been noted in most ETME sections (Thibodeau et al., 2016; Percival et al., 2017; Yager et al., 2021; Schoepfer et al., 2022; Shen et al., 2022a, 2022b) – the St Audrie's Bay data in this study and Hua et al. (2023) notwithstanding. In detail, however, Hg enrichment magnitudes across the ETME have not been quantitively and statistically evaluated, either stratigraphically or between study locations. As such, the true significance of Hg enrichment across the ETME, and its links to volcanism, is unclear.

At St Audrie's Bay, the correlation heatmaps between Hg and whole-

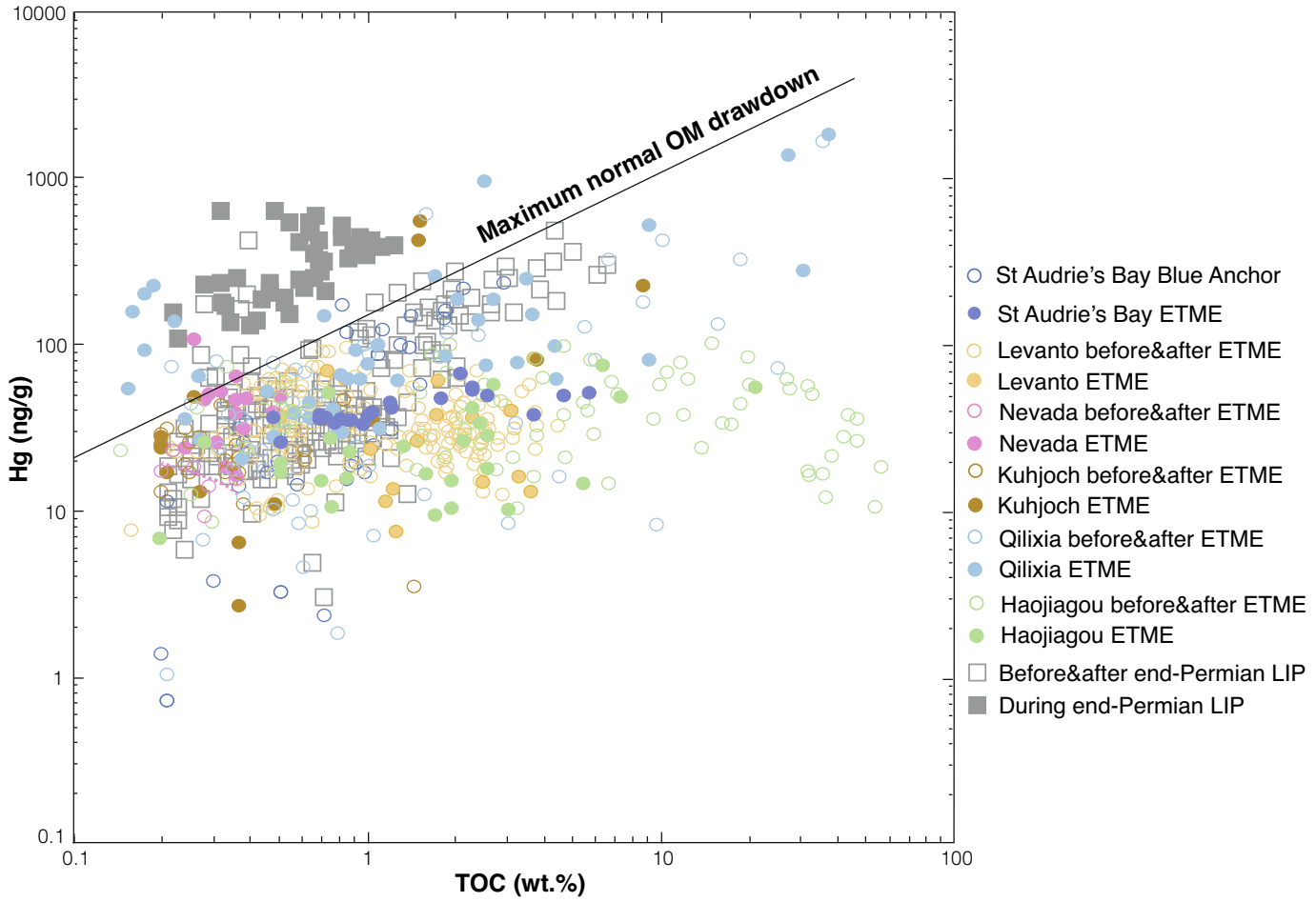

Fig. 7. Plot of Hg versus TOC from the studied end-Triassic sections. Data from the ETME interval of each section are separated from the data before & after ETME intervals (background interval). The line of maximum likely organic matter (OM) drawdown (solid black line) is defined by the power law equation: Hg = 150 $TOC^{0.83}$, as proposed by Grasby et al. (2019). Data sources: St Audrie's Bay from Hua et al. (2023), Levanto from Yager et al. (2021), New York Canyon from Thibodeau et al. (2016), Kuhjoch from Percival et al. (2017), Qilixia and Haojiagou from Shen et al. (2022a), end-Permian data from Grasby et al. (2016). LIP: large igneous province.

rock geochemistry (Fig. 2) help to show how dominant Hg host phases vary stratigraphically, allowing for more nuanced and robust recognition of Hg anomalies related potentially to exogenic volcanic input. However, linear regression on its own has the issue that the magnitude and significance of a potential anomaly relative to the rest of the data are not clear.

Here, a new way to quantify Hg anomalies using whole-rock correlation analysis is established based on calculation of externally studentized residuals (Cook and Weisberg, 1982, also known as studentized deleted residuals). This method is exceptionally suitable for identifying outliers and assessing their relative magnitude. In linear regression analysis, a studentized residual is calculated by dividing a residual by an estimate of its standard deviation, thus yielding a standardized ('studentized') value. For externally studentized residuals, the regression model from which a residual is calculated is fitted without the observation in question (i.e. it is deleted from the regression model). Hence:

$$t_i = \frac{d_i}{s(d)_i} = \frac{e_i}{\sqrt{MSE_{(i)}\left(1 - h_{ii}\right)}},$$

where the externally studentized residual (t_i) is calculated by dividing the deleted residual (d_i) by its estimated standard deviation ($s(d)_i$), which is equal to dividing the ordinary residual (e_i) by a quantity that incorporates the mean square error derived from the regression model excluding the ith observation ($MSE_{(i)}$), and the leverage (h_{ii}), which is a measure of the extremity of the x-axis value (independent variable) for the residual in question.

The key justification for using externally studentized residuals is that if a true outlier (i.e. anomaly) exists in a dataset, then this would have the effect of pulling the regression slope towards it, thus compromising the accuracy of the linear regression model for all other samples, and reducing the true residual size of the outlier. Thus, stratigraphical outliers in Hg concentration can be estimated compared to the major Hg host phases or other whole-rock geochemical data. Nevertheless, Hg concentration variations resulting from the contribution of multiple host phases are not accounted for, as the method assesses only one pair of variables (Hg and some other geochemical component) at a time.

Geochemical data that have at least moderate and significant coefficients of determination with Hg ($R^2 > 0.3$, i.e. $r > 0.547$, $p < 0.01$) are selected for the externally studentized residual calculations. The externally studentized residuals for each sample can be plotted onto a heatmap to better visualize the anomalies among different samples and elements through a section (Fig. 8). In general statistical practice, outliers (i.e. anomalies) can be defined as those with externally studentized residual values >3 (the "3-sigma rule"). With this method, a sample exhibiting a true Hg anomaly that is associated with an anomalous Hg input (i.e. volcanism) rather than host phase variation should yield consistently high externally studentized residual values when normalized to the correct host phase and other elements associated with that host phase (e.g., a sample with externally studentized residuals >3 with respect to Al and other elements with clay mineral affinity).

Table 1
Regression equations, Pearson correlation coefficients and significance level between Hg and TOC in the studied sections.

Section	Regression Equation	Correlation coefficients	Data sources
St Audrie's Bay			This study
Before ETME (Blue Anchor Formation)	$y = 89.52x - 22.18$	$r = 0.85$, $p < 0.01$, $n = 39$	
Within ETME	$y = 3.84x + 35.26$	$r = 0.57$, $p < 0.01$, $n = 22$	
Levanto			Yager et al., 2021
Before & after ETME	$y = -1.87x + 37.45$	$r = -0.10$, $p = 0.17$, $n = 178$	
Within ETME	$y = 0.11x + 34.25$	$r = 0.004$, $p = 0.99$, $n = 16$	
New York Canyon			Thibodeau et al., 2016
Before & after ETME	$y = -38.88x + 26.70$	$r = -0.47$, $p = 0.35$, $n = 6$	
Within ETME	$y = -9.67x + 45.93$	$r = -0.35$, $p = 0.18$, n = 16	
Kuhjoch			Percival et al., 2017
Before & after ETME	$y = -7.53x + 26.07$	$r = -0.22$, $p = 0.32$, n = 22	
Within ETME	$y = 24.64x + 73.19$	$r = 0.33$, $p = 0.25$, $n = 14$	
Qilixia			Shen et al., 2022a
Before & after ETME	$y = 26.73x + 15.11$	$r = 0.44$, $p < 0.01$, $n = 52$	
Within ETME	$y = 34.93x + 65.97$	$r = 0.79$, $p < 0.01$, $n = 45$	
Haojiagou			Shen et al., 2022a
Before & after ETME	$y = -0.30x + 45.80$	$r = 0.06$, $p = 0.72$, $n = 37$	
Within ETME	$y = 2.19x + 20.68$	$r = 0.51$, $p < 0.01$, $n = 26$	

In our analysis of the St. Audrie's Bay dataset, we observe that the maximum Hg residuals in the Blue Anchor Formation are larger than in other intervals (Fig. 8). However, there are no samples with consistently high Hg anomalies (i.e. with externally studentized residuals >3) for multiple whole rock elements/components associated with the different potential host phases in the Blue Anchor Formation. For instance, Hg concentrations are high in sample B35 (22.7 m height), and this sample shows anomalies (externally studentized residual values >3) with respect to Fe (3.8), Co (4.7), Ni (3.7), As (3.4), Ag (3.4) and Pb (3.1) (Fig. 8). However, no significant anomaly exists with respect to organic matter (TOC) or sulfide, which are the likely dominant host phases in this formation (Fig. 8; Section 5.1). By contrast, the relatively high Hg in sample B19 (5.9 m height) is associated with a significant anomaly with respect to TOC (4.2, and also slightly enriched with respect to sulfide), but covaries with other trace elements without any externally studentized residual values >3. In the Westbury Formation, Hg is relatively enriched in samples W9 and W24 (33.1 and 36.85 m height, respectively). However, anomalies >3 exist only with respect to Cu (3.1) in W9, and Fe (3.3) and Bi (3.1) in W24, respectively (Fig. 8). Similarly, no consistent anomalies exist within the Lilstock Formation and Blue Lias Formation (Fig. 8). Samples W46 and W54 have relatively high Hg. W46 (42.35 m height) has an externally studentized residual of 3.2 with respect to Cd, and 3.4 with respect to Tl. Sample W54 (44.35 m height) has externally studentized residuals of 3.4, 3.0, 3.1 with respect to Cu, Sn and Sb, respectively. Importantly, however, no consistent clear anomalies exist with respect to other elements with sulfide/clay affinity across these formations. In addition, externally studentized residual are also calculated based on the Hg and TOC data of St Audrie's Bay from Percival et al. (2017). The result also shows that no externally studentized residuals >3 occur across the ETME interval (Fig. 9 and Fig. 10).

5.4. Critical evaluation of possible paleo-volcanism signals across the end-Triassic

Our novel approach of using externally studentized residuals to quantify Hg anomalies can be applied to the other end-Triassic successions (Fig. 9; Fig. 10). This exercise shows that, in contrast to St Audrie's Bay, Hg anomalies do exist across the ETME interval in the other compiled sections (Figs. 9 and 10) – albeit with the caveat that these sections generally lack data for multiple potential host phases/whole rock components (see Section 5.2).

At Kuhjoch, Hg anomalies based on externally studentized residual calculations have values of up to 11.1 during the inferred Marshi NCIE, but no other anomalies in the ETME interval occur above this (Figs. 9 and 10). At New York Canyon, an anomaly (4.9) occurs above the Spelae CIE within the ETME, while at Levanto anomalies (maximum of 3.6) occur near the top of ETME interval in the inferred Spelae NCIE and above. The anomalies in these sections are quantified with respect to TOC (Table 1), and although organic matter may not be the main host in these sections (Section 5.2), the occurrence of anomalies in the ETME contrasts with the absence of any anomalies at St. Audrie's Bay. Two intervals of anomalies occur at Qilixia, likely close to the Marshi NCIE (maximum of 4.9) and the Spelae NCIE (maximum of 4.0) respectively (Figs. 9 and 10). At Haojiagou, two smaller anomalies (maximum of 2.91) occur across the Spelae NCIE (Figs. 9 and 10). At the Kurusu and Katsuyama sections in Japan, anomalies exist (maxima of 3.92 and 8.33, respectively) with respect to the identified host phase of non-acid volatile sulfur (NAVS) and clay fraction (represented by Th), respectively. These anomalies occur across the inferred Spelae NCIE (Figs. 9 and 10).

The lack of any Hg anomaly across the ETME interval at St Audrie's Bay is consistent with the findings of Hua et al. (2023), but is statistically demonstrated here. Sedimentary factors could possibly contribute to the result at St Audrie's Bay. Notably, as discussed in Section 5.1, low HI and high OI values across the ETME indicate possible Hg loss caused by alteration/oxidation of organic matter (Fig. 6). This could have prevented clear expression of any anomalies. Secondly, the oversupply of host phases (i.e. clays and sulfide, indicated by the correlation slopes, Fig. 5) relative to Hg within the Westbury to Blue Lias Formations could further explain why Hg/host phase shows negligible changes across the ETME interval, even if the Hg flux there does include a volcanic component. Indeed, Hua et al. (2023) clearly demonstrated (using Hg isotope analysis) the likelihood that Hg in the St. Audrie's Bay section was sourced from magmatism. In this scenario, therefore, the oversupply of host phases ensures low Hg/host values, even though it is probable that exogenic Hg entered the basin via atmospheric deposition. This result indicates that the slope of any correlation between Hg and a potential host should be taken into consideration for determining if Hg anomaly signals can be recognized in a given section. Hua et al. (2023) speculated that the absence of Hg anomalies at St. Audrie's Bay could have also been related to the rapid cycling that this element undergoes during atmospheric transport (residence time of 0.5–2 years), weakening its potential enrichment even in basins geographically proximal to volcanic sources. Quantification of the amount of Hg required to drive the observed changes in Hg isotopes at St. Audrie's Bay by Hua et al. (2023) suggested that Hg fluxes to St. Audrie's Bay may have been low relative to the amount of Hg likely released by CAMP, thus limiting the possibility of preserving a clear Hg anomaly. In addition, the atmospheric deposition of Hg could be further limited by climate factors. For instance, during the drier, low rainfall conditions that may have characterized the ETME at St. Audrie's Bay (Bonis et al., 2010), atmospheric wet deposition would have been weakened.

Fig. 10 highlights how the relationship between Hg enrichments and Hg isotope records also vary globally (Fig. 10). In theory, changes in Hg flux could affect Hg concentration as well as Hg isotopes if the Hg source varies. At St. Audrie's Bay, the Hg isotope record (mass independent fractionation, expressed via Δ^{199}Hg) shows successive negative-positive Δ^{199}Hg shifts that were attributed to thermogenic release from CAMP

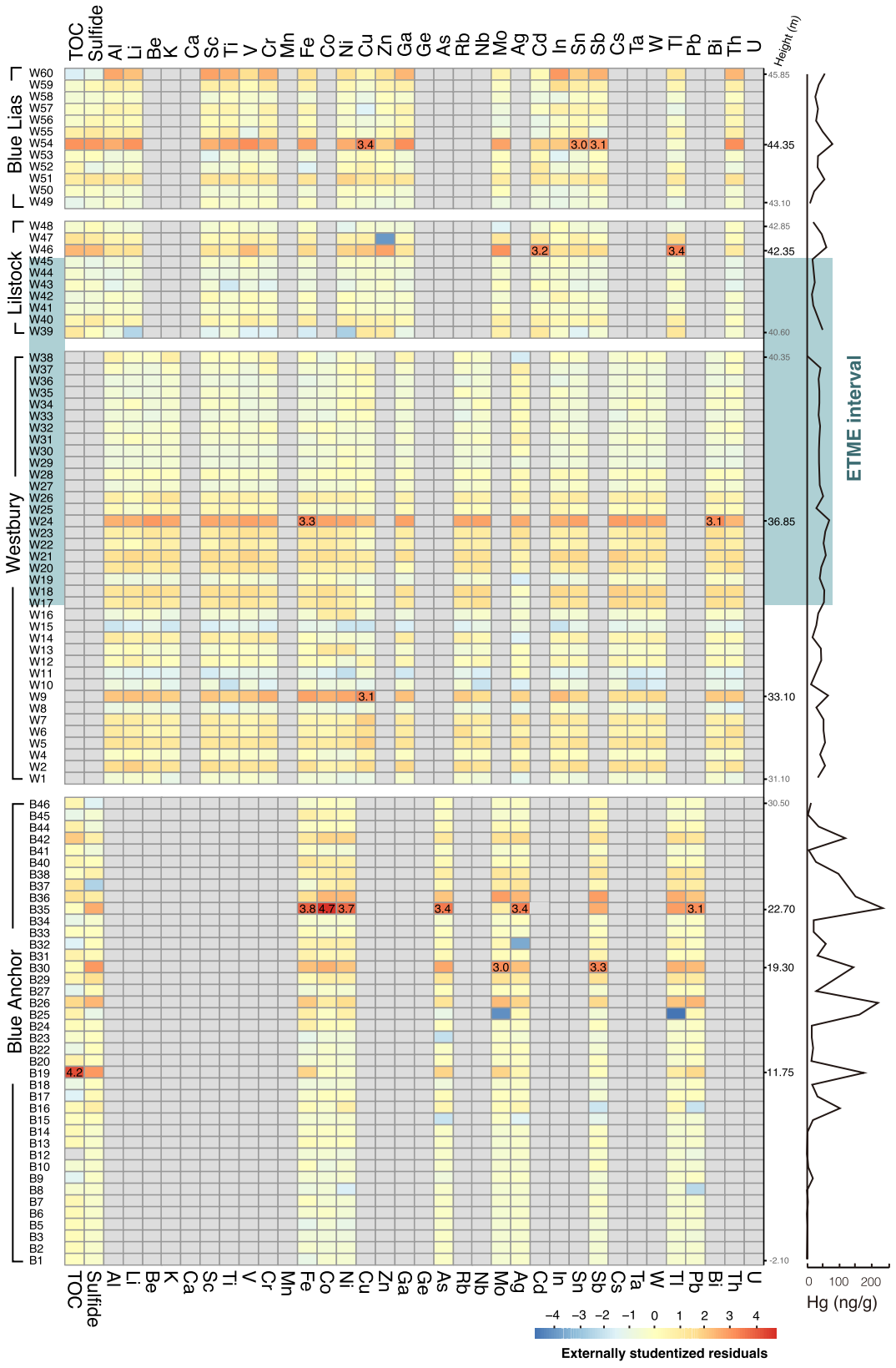

Fig. 8. Heatmap of Hg anomalies across St. Audrie's Bay, based on externally studentized residual calculation. Only data with an Hg–component coefficient of determination (R^2) of >0.3 are shown (grey boxes represent elements not used as the correlation with Hg was <0.3). Box colour represents Hg residual magnitude. Anomalies (externally studentized residual values) >3 are indicated, and the heights of these also shown. Green-shaded area indicates the ETME interval. (For interpretation of the references to colour in this figure legend, the reader is referred to the web version of this article.)

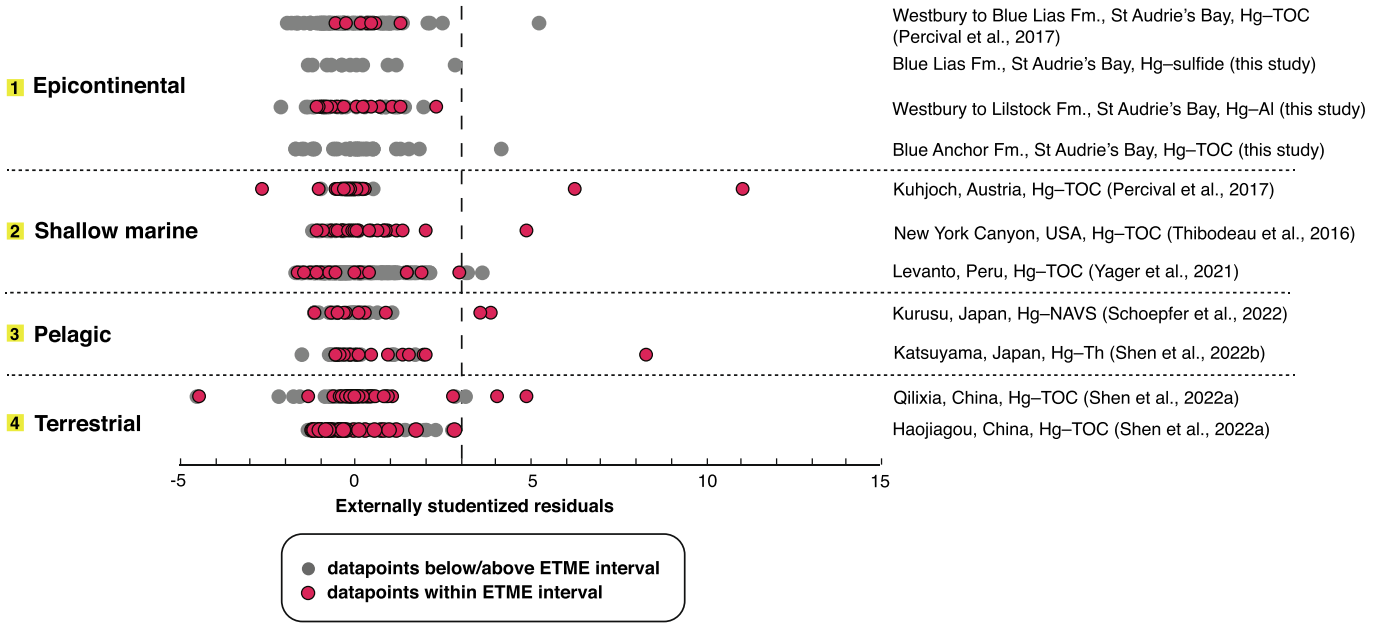

Fig. 9. Global comparison of Hg anomalies across the ETME at different sites/depositional environments. Anomalies were calculated as externally studentized residuals based on correlation between Hg and the inferred host phase (see main text for details). For the St. Audrie's Bay data, Hg–TOC in the Blue Anchor Formation (in purple colour), Hg—Al in the Westbury and Lilstock formations (in orange colour), and Hg–Sulfide in the Blue Lias Formation (in grey colour). Anomaly calculation for the Hg–TOC data of Percival et al. (2017) are also shown for comparison (in red colour). Anomaly calculation for Kuhjoch based on Hg–TOC (Percival et al., 2017). Anomaly calculation for New York Canyon based on Hg–TOC (Thibodeau et al., 2016). Anomaly calculation for Levanto based on Hg–TOC (Yager et al., 2021). Anomaly calculation for Kurusu based on Hg–nonacid volatile sulfur (NAVS) (Schoepfer et al., 2022). Anomaly calculation for Katsuyama based on Hg—Th (Shen et al., 2022b). Anomaly calculation for Qilixia based on Hg–TOC (Shen et al., 2022a). Anomaly calculation for Haojiagou based on Hg–TOC (Shen et al., 2022a). (For interpretation of the references to colour in this figure legend, the reader is referred to the web version of this article.)

intrusions heating organic rich sediments (causing the negative shift), followed by mantle-sourced volcanic release (causing the positive shift; Fig. 10; Hua et al., 2023). However, there is no correlation between Hg/host phase and Δ^{199}Hg across the ETME, and consequently no correlation between externally studentized residual values and Δ^{199}Hg either (Fig. 10; Fig. S3a). Similarly, there is no significant correlation between externally studentized residual values and Δ^{199}Hg at the other shelf shallow marine sections of New York Canyon ($r = 0.01$, $p = 0.95$; Fig. 10; Fig. S3b; Thibodeau et al., 2016) and Levanto ($r = -0.24$, $p = 0.33$; Fig. 10; Fig. S3c; Yager et al., 2021). There is an insignificant negative relationship ($r = -0.48$, $p = 0.18$) between calculated residuals and negative shifts in Δ^{199}Hg at Katsuyama (Fig. 10; Fig. S3d). Here, a negative Δ^{199}Hg shift (Fig. 10) was attributed to thermogenic release from CAMP magmatic heating organic rich sediments at this remote oceanic location with limited terrestrial signal (Shen et al., 2022b). At Qilixia and Haojiagou, several Hg anomaly spikes across the ETME correspond with Δ^{199}Hg negative shifts, although the Δ^{199}Hg–residual correlations are again not significant ($r = 0.25$, $p = 0.36$ at Qilixia, $r = 0.31$, $p = 0.26$ at Haojiagou; Shen et al., 2022a; Fig. 9; Fig. S3e and S3f). The negative shifts in Δ^{199}Hg at Qilixia and Haojiagou sections may have resulted from increased terrestrial Hg input with negative Δ^{199}Hg arising from intensive chemical weathering related to magmatic carbon release and warming (Shen et al., 2022a).

The paleo-volcanism signals found in the globally distributed ETME sections based on our new method of Hg anomaly calculation occur within or at least close to the ETME, and often coincident with CIEs, but were clearly asynchronous (Fig. 10). Thus, although the data suggest these Hg anomalies could be indicative of paleo-volcanism, it is likely that at these sites, as at St. Audrie's Bay, other factors were important in determining the precise timing and magnitude of Hg enrichment.

6. Conclusions

The St Audrie's Bay section provides a unique opportunity to test the efficacy of the Hg as paleo-volcanism proxy and establish the environmental controls on Hg abundance in ancient sedimentary strata. Hg host phases vary through the Late Triassic to Early Jurassic interval with changing depositional environments. Depositional controls such as the supply of host phase contents, and *syn*-depositional controls such as subaerial exposure and oxidation, are important controls on relative Hg abundance in this section. Hg anomaly calculation based on externally studentized residuals provides a robust way to evaluate Hg anomalies for use in paleo-volcanism studies. Applying this method reveals no clear Hg anomalies in any part of the St. Audrie's Bay succession that could be attributed to magmatism, despite recent Hg isotope evidence for both volcanic and thermogenic Hg release. However, other (globally distributed) Late Triassic sections do show clear evidence for Hg anomalies across the ETME, although Hg was likely undersupplied relative to the important host phase of organic matter. Taken together, care needs to be taken to establish the sedimentary controls on Hg signals before application of the Hg paleo-volcanism proxy, but this in itself is no guarantee that an individual section will record Hg with the fidelity required to identify volcanic inputs of Hg.

CRediT authorship contribution statement

Xia Hua: Writing – original draft, Methodology, Investigation, Formal analysis, Data curation, Conceptualization. **David B. Kemp:** Writing – review & editing, Supervision, Funding acquisition, Formal analysis, Conceptualization. **Jun Shen:** Writing – review & editing, Validation. **Runsheng Yin:** Writing – review & editing, Resources. **Xin Jin:** Writing – review & editing, Formal analysis. **Chunju Huang:** Supervision, Funding acquisition.

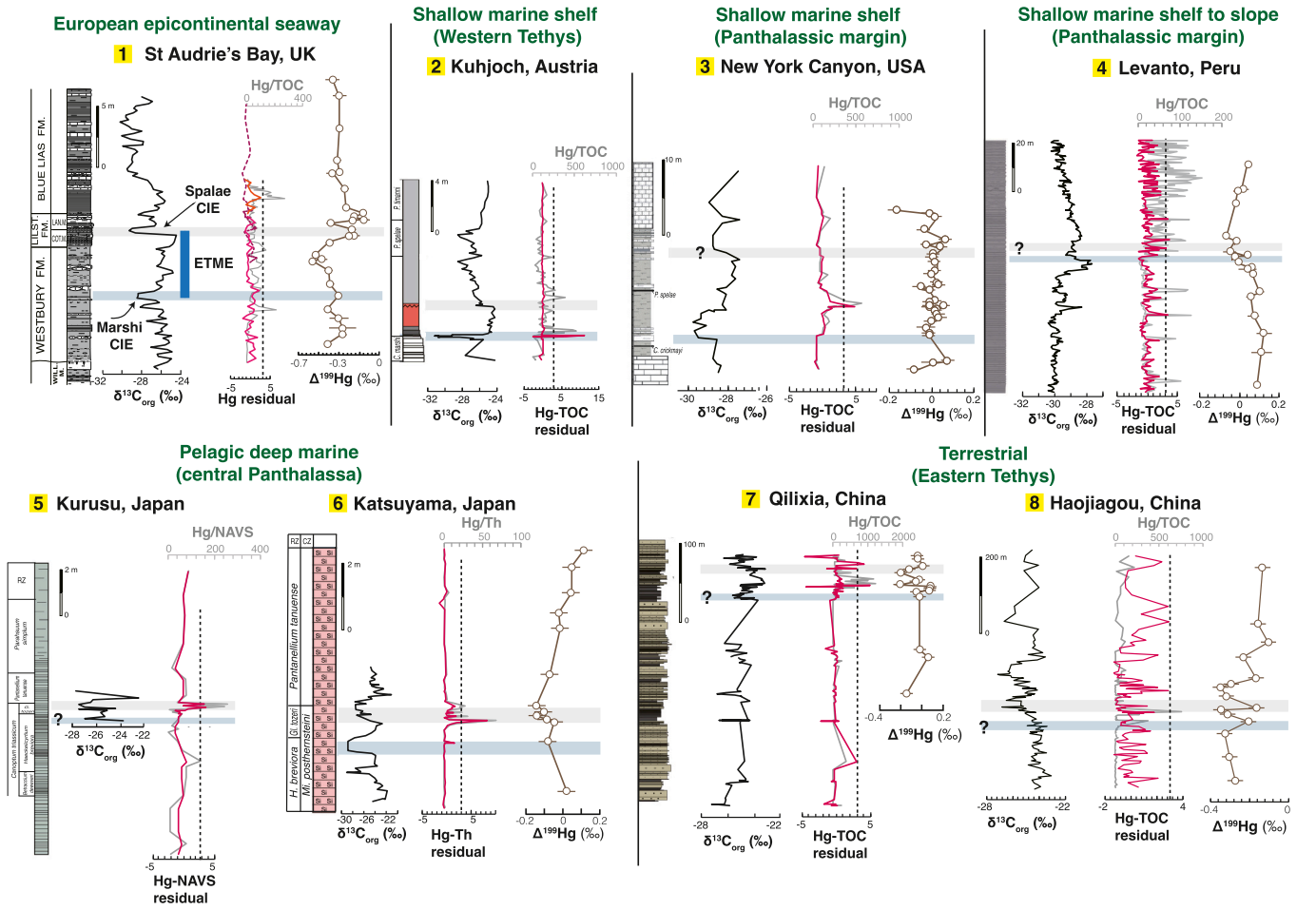

Fig. 10. Stratigraphic comparison of global Hg anomalies, C isotopes and Hg isotopes across the ETME at different sites/depositional environments. Data are the same as those plotted in Fig. 9. Lithology of Kuhjoch is from Percival et al. (2017), New York Canyon from Thibodeau et al. (2016), Levanto from Yager et al. (2021), Kurusu from Schoepfer et al. (2022), Katsuyama from Shen et al. (2022b), Qilixia and Haojiagou from Shen et al. (2022a). Grey lines indicate Hg/host in each section. Red lines indicate calculated Hg anomaly with respect to the host in each section. At St Audrie's Bay, the red dashed line indicates the calculated Hg anomaly with respect to TOC (data from Percival et al., 2017). The red line indicates the calculated Hg anomaly with respect to Al in the Westbury and Lilstock formations. The orange line indicates the calculated Hg anomaly with respect to sulfide in the Blue Lias Formation. Carbon isotope data for St Audrie's Bay are from Hesselbo et al. (2002), for Kuhjoch from Ruhl et al. (2009), for New York Canyon from (Thibodeau et al., 2016), for Levanto from (Yager et al., 2017), for Kurusu from Kuroda et al. (2010), for Katsuyama from Fujisaki et al. (2018), and for Qilixia and Haojiagou from Shen et al. (2022a). Hg isotope data for St Audrie's Bay are from Hua et al. (2023), for New York Canyon from Thibodeau et al. (2016), for Levanto from Yager et al. (2021), for Katsuyama from Shen et al. (2022b), and for Qilixia and Haojiagou from Shen et al. (2022a). Anomalies (externally studentized residual values) >3 are recognized as true anomalies potentially indicative of exogenic Hg input (i.e. volcanism, see main text for details). ETME interval (definition following Lindström et al., 2021) is shown as a blue bar. Section locations (yellow numbers next to each site name) are shown in Fig. 1. (For interpretation of the references to colour in this figure legend, the reader is referred to the web version of this article.)

Declaration of competing interest

The authors declare that they have no known competing financial interests or personal relationships that could have appeared to influence the work reported in this paper.

Data availability

Data will be made available on request.

Acknowledgement

This work was supported by the National Natural Science Foundation of China (Grant No. 42230208, 42272033, 42488201, 42172039). This work is a contribution to IGCP 739.

Appendix A. Supplementary data

Supplementary data to this article can be found online at https://doi.org/10.1016/j.gloplacha.2024.104589.

References

Algeo, T.J., Tribovillard, N., 2009. Environmental analysis of paleoceanographic systems based on molybdenum–uranium covariation. Chem. Geol. 268 (3–4), 211–225.
Blackburn, T.J., Olsen, P.E., Bowring, S.A., McLean, N.M., Kent, D.V., Puffer, J., McHone, G., Rasbury, E.T., Et-Touhami, M., 2013. Zircon U-Pb geochronology links the end-Triassic extinction with the Central Atlantic Magmatic Province. Science 340 (6135), 941–945.
Bonis, N.R., Kürschner, W.M., Krystyn, L., 2009. A detailed palynological study of the Triassic–Jurassic transition in key sections of the Eiberg Basin (Northern Calcareous Alps, Austria). Rev. Palaeobot. Palynol. 156, 376–400.
Bonis, N.R., Ruhl, M., Kürschner, W.M., 2010. Milankovitch-scale palynological turnover across the Triassic–Jurassic transition at St. Audrie's Bay, SW UK. J. Geol. Soc. Lond. 167 (5), 877–888.

Bos, R., Zheng, W., Lindström, S., Sanei, H., Waajen, I., Fendley, I.M., Mather, T.A., Wang, Y., Rohovec, J., Navrátil, T., Sluijs, A., van de Schootbrugge, B., 2024. Climate-forced Hg-remobilization associated with fern mutagenesis in the aftermath of the end-Triassic extinction. Nat. Commun. 15 (1), 3596.
Bower, J., Savage, K.S., Weinman, B., Barnett, M.O., Hamilton, W.P., Harper, W.F., 2008. Immobilization of mercury by pyrite (FeS_2). Environ. Pollut. 156 (2), 504–514.
Calvert, S.E., Pedersen, T.F., 2007. Chapter fourteen elemental proxies for palaeoclimatic and palaeoceanographic variability in marine sediments: interpretation and application. Dev. Mar. Geol. 1, 567–644.
Charbonnier, G., Adatte, T., Föllmi, K.B., Suan, G., 2020. Effect of intense weathering and postdepositional degradation of organic matter on Hg/TOC proxy in organic-rich sediments and its implications for deep-time investigations. Geochem. Geophys. Geosyst. 21.
Cook, R.D., Weisberg, S., 1982. Residuals and Influence in Regression.
Davies, J., Marzoli, A., Bertrand, H., Youbi, N., Ernesto, M., Schaltegger, U., 2017. End-Triassic mass extinction started by intrusive CAMP activity. Nat. Commun. 8, 15596.
Erickson, B.E., Helz, G.R., 2000. Molybdenum (VI) speciation in sulfidic waters: stability and lability of thiomolybdates. Geochim. Cosmochim. Acta 64, 1149–1158.
Espitalié, J., Deroo, G., Marquis, F., 1985. La pyrolyse Rock-Eval et ses applications. Revue l'Institut Français du Pétrol 40 (5), 563–579.
Farrah, H., Pickering, W.F., 1978. The sorption of mercury species by clay minerals. Water Air Soil Pollut. 9, 23–31.
Fox, C., Cui, X., Whiteside, J.H., Olsen, P.E., Summons, R.E., Grice, K., 2020. Molecular and isotopic evidence reveals the end-Triassic carbon isotope excursion is not from massive exogenous light carbon. Proc. Natl. Acad. Sci. 117 (48), 30171–30178.
Fujisaki, W., Matsui, Y., Asanuma, H., Sawaki, Y., Suzuki, K., Maruyama, S., 2018. Global perturbation of carbon cycle during the Triassic-Jurassic transition recorded in the mid-Panthalassa. Earth Planet. Sci. Lett. 500, 105–116.
Grasby, S.E., Beauchamp, B., Bond, D.P.G., Wignall, P.B., Sanei, H., 2016. Mercury anomalies associated with three extinction events (Capitanian Crisis, latest Permian Extinction and the Smithian/Spathian Extinction) in NW Pangea. Geol. Mag. 153 (2), 285–297.
Grasby, S.E., Shen, W., Yin, R., Gleason, J.D., Blum, J.D., Lepak, R.F., Hurley, J.P., Beauchamp, B., 2017. Isotopic signatures of mercury contamination in latest Permian oceans. Geology 45 (1), 55–58.
Grasby, S.E., Them II, T.R., Chen, Z., Yin, R.S., Ardakani, O.H., 2019. Mercury as a proxy for volcanic emissions in the geologic record. Earth Sci. Rev. 196, 102880.
Gregory, D.D., Large, R.R., Halpin, J.A., Baturina, E.L., Lyons, T.W., Wu, S., Danyushevsky, L., Sack, P.J., Chappaz, A., Maslennikov, V.V., Stuart, W., Bull, S.W., 2015. Trace element content of sedimentary pyrite in black shales. Econ. Geol. 110 (6), 1389–1410.
Hallam, A., 2001. A review of the broad pattern of Jurassic sea-level changes and their possible causes in the light of current knowledge. Paleogeogr. Paleoclimatol. Paleoecol. 167 (1–2), 23–37.
He, T., Wignall, P.B., Newton, R.J., Atkinson, J.W., Keeling, J.F., Xiong, Y., Poulton, S. W., 2022. Extensive marine anoxia in the European epicontinental sea during the end-Triassic mass extinction. Glob. Planet. Chang. 210, 103771.
Hesselbo, S.P., Robinson, S.A., Surlyk, F., Piasecki, S., 2002. Terrestrial and marine extinction at the Triassic-Jurassic boundary synchronized with major carbon-cycle perturbation: a link to initiation of massive volcanism? Geology 30, 251–254.
Hesselbo, S.P., Robinson, S.A., Surlyk, F., 2004. Sea-level changes and facies development across potential Triassic-Jurassic boundary horizons, SW Britain. J. Geol. Soc. Lond. 161, 365–379.
Hillebrandt, A.V., Krystyn, L., Kuerschner, W., Bown, P., Mcroberts, C., Ruhl, M., Simms, M., Tomašovỳch, A., Urlichs, M., 2007. A candidate GSSP for the base of the Jurassic in the Northern Calcareous Alps (Kuhjoch section, Karwendel Mountains, Tyrol, Austria). ISJS 34, 2–20.
Hillebrandt, A.V., Krystyn, L., Kurschner, W.M., Bonis, N.R., Ruhl, M., Richoz, S., Schobben, M.A.N., Urlichs, M., Bown, P.R., Kment, K., McRoberts, C.A., Simms, M., Tomasovych, A., 2013. The Global Stratotype Sections and Point (GSSP) for the base of the Jurassic system at Kuhjoch (Karwendel Mountains, Northern Calcareous Alps, Tyrol, Austria). Episodes 36, 162–198.
Hua, X., Yin, R., Kemp, D.B., Huang, C., Shen, J., Jin, X., 2023. Mercury isotope constraints on the timing and pattern of magmatism during the end-Triassic mass extinction. Earth Planet. Sci. Lett. 624, 118438.
Ikeda, M., Tada, R., 2014. A 70 million year astronomical time scale for the deep-sea bedded chert sequence (Inuyama, Japan): Implications for the Triassic-Jurassic geochronology. Earth Planet. Sci. Lett. 399, 30–43.
Ikeda, M., Tada, R., Ozaki, K., 2017. Astronomical pacing of the global silica cycle recorded in Mesozoic bedded cherts. Nat. Commun. 8, 15532.
Ivimey-Cook, H.C., Hodges, P., Swift, A., Radley, J.D., 1999. Bivalves. In: Swift, A., Martill, D.M. (Eds.), Fossils of the Rhaetian Penarth Group. The Palaeontological Association, pp. 83–128.
Jin, X., Ogg, J.G., Lu, S., Shi, Z., Kemp, D.B., Hua, X., Onoue, T., Rigo, M., 2022. Terrestrial record of carbon-isotope shifts across the Norian/Rhaetian boundary: a high-resolution study from northwestern Sichuan Basin, South China. Glob. Planet. Chang. 210, 103754.
Kersten, M., Forstner, U., 1989. Speciation of trace elements in sediments. In: Trace Element Speciation: Analytical Methods and Problems, pp. 245–317.
Kongchum, M., Hudnall, W.H., Delaune, R.D., 2011. Relationship between sediment clay minerals and total mercury. J. Environ. Sci. Health A 46 (5), 534–539.
Korte, C., Hesselbo, S.P., Jenkyns, H.C., Rickaby, R.E.M., Spotl, C., 2009. Palaeoenvironmental significance of carbon- and oxygen-isotope stratigraphy of marine Triassic-Jurassic boundary sections in SW Britain. J. Geol. Soc. Lond. 166, 431–445.
Kovács, E.B., Ruhl, M., Silva, R.L., McElwain, J.C., Reolid, M., Korte, C., Ruebsam, W., Hesselbo, S.P., 2024. Mercury sequestration pathways under varying depositional conditions during early Jurassic (Pliensbachian and Toarcian) Karoo-Ferrar volcanism. Palaeogeogr. Palaeoclimatol. Palaeoecol. 637, 111977.
Kuroda, J., Hori, R.S., Suzuki, K., Grocke, D., Ohkouchi, N., 2010. Marine osmium isotope record across the Triassic-Jurassic boundary from a Pacific pelagic site. Geology 38, 1095–1098.
Li, L., Wang, Y., Kürschner, W.M., Ruhl, M., Vajda, V., 2020. Palaeovegetation and palaeoclimate changes across the Triassic–Jurassic transition in the Sichuan Basin, China. Paleogeogr. Paleoclimatol. Paleoecol. 556, 109891.
Lindström, S., van de Schootbrugge, B., Hansen, K.H., Pedersen, G.K., Alsen, P., Thibault, N., Dybkjær, K., Bjerrum, C.J., Nielsen, L.H., 2017. A new correlation of Triassic-Jurassic boundary successions in NW Europe, Nevada and Peru, and the Central Atlantic Magmatic Province: a time-line for the end-Triassic mass extinction. Palaeogeogr. Palaeoclimatol. Palaeoecol. 478, 80–102.
Lindström, S., Sanei, H., van de Schootbrugge, B., Pedersen, G.K., Lesher, C.E., Tegner, C., Heunisch, C., Dybkjær, K., Outridge, P.M., 2019. Volcanic mercury and mutagenesis in land plants during the end-Triassic mass extinction. Sci. Adv. 5, eaaw4018.
Lindström, S., Callegaro, S., Davies, J., Tegner, C., van de Schootbrugge, B., Pedersen, G., Youbi, N., Sanei, H., Marzoli, A., 2021. Tracing volcanic emissions from the Central Atlantic Magmatic Province in the sedimentary record. Earth Sci. Rev. 212, 103444.
Lucas, S.G., Taylor, D.G., Guex, J., Tanner, L.H., Krainer, K., 2007. The proposed global stratotype section and point for the base of the Jurassic System in the New York Canyon area, Nevada, USA. N. M. Mus. Nat. Hist. Sci. Bull. 40, 139–168.
Macquaker, J.H.S., 1987. The Depositional and Diagenetic History of the Westbury Formation (Upper Triassic) in South West Britain (Doctoral dissertation,. University of Bristol.
Mayall, M.J., 1981. The Late Triassic Blue Anchor Formation and the initial Rhaetian marine transgression in south-West Britain. Geol. Mag. 118, 377–384.
Morse, J.W., Luther III, G.W., 1999. Chemical influences on trace metal-sulfide interactions in anoxic sediments. Geochim. Cosmochim. Acta 63 (19–20), 3373–3378.
Mostofa, K.M.G., Liu, C.Q., Feng, X., Yoshioka, T., Vione, D., Pan, X., Wu, F., 2013. Complexation of dissolved organic matter with trace metal ions in natural waters. In: Photobiogeochemistry of Organic Matter: Principles and Practices in Water Environments, pp. 769–849.
Oliveri, E., Sprovieri, M., Manta, D.S., Giaramita, L., La Cono, V., Lirer, F., Rumolo, P., Sabatino, N., Tranchida, G., Vallefuoco, M., Yakimov, M.M., Mazzola, S., 2013. Sediment geochemistry of the Thetis hypersaline anoxic basin (eastern Mediterranean Sea). Sediment. Geol. 296, 72–85.
Park, J., Stein, H., Georgiev, S., Hannah, J., 2022. Degradation of Hg signals on incipient weathering: core versus outcrop geochemistry of Upper Permian shales, East Greenland and Mid-Norwegian Shelf. Chem. Geol. 608, 121030.
Percival, L.M., Ruhl, M., Hesselbo, S.P., Jenkyns, H.C., Mather, T.A., Whiteside, J.H., 2017. Mercury evidence for pulsed volcanism during the end-Triassic mass extinction. Proc. Natl. Acad. Sci. 114, 7929–7934.
Querol, X., Fernández-Turiel, J., López-Soler, A., 1995. Trace elements in coal and their behaviour during combustion in a large power station. Fuel 74 (3), 331–343.
Ravichandran, M., 2004. Interactions between mercury and dissolved organic matter—a review. Chemosphere 55, 319–331.
Ruhl, M., Kürschner, W.M., 2011. Multiple phases of carbon cycle disturbance from large igneous province formation at the Triassic-Jurassic transition. Geology 39, 431–434.
Ruhl, M., Kürschner, W.M., Krystyn, L., 2009. Triassic-Jurassic organic carbon isotope stratigraphy of key sections in the western Tethys realm (Austria). Earth Planet. Sci. Lett. 281, 169–187.
Ruhl, M., Bonis, N.R., Reichart, G.J., Damsté, J.S.S., Kürschner, W.M., 2011. Atmospheric carbon injection linked to end-Triassic mass extinction. Science 333 (6041), 430–434.
Sanei, H., Grasby, S.E., Beauchamp, B., 2012. Latest Permian mercury anomalies. Geology 40, 63–66.
Sanei, H., Outridge, P.M., Stern, G.A., Macdonald, R.W., 2014. Classification of mercury–labile organic matter relationships in lake sediments. Chem. Geol. 373, 87–92.
Schoepfer, S.D., Algeo, J.T., van de Schootbrugge, B., Whiteside, J.H., 2022. The Triassic-Jurassic transition – a review of environmental change at the dawn of the modern life. Earth Sci. Rev. 232, 104099.
Selin, N.E., 2009. Global biogeochemical cycling of mercury: a review. Annu. Rev. Environ. Resour. 34, 43–63.
Shen, J., Algeo, T.J., Planavsky, N.J., Yu, J.X., Feng, Q.L., Song, H.J., Song, H.Y., Rowe, H., Zhou, L., Chen, J.B., 2019a. Mercury enrichments provide evidence of early Triassic volcanism following the end-Permian mass extinction. Earth Sci. Rev. 195, 191–212.
Sha, J., Vajda, V., Pan, Y., Larsson, L., Yao, X., Zhang, X., Wang, Y., Cheng, X., Jiang, B., Deng, S., Chen, S., Peng, B., 2011. Stratigraphy of the Triassic–Jurassic boundary successions of the southern margin of the Junggar Basin, northwestern China. Acta Sedimentol. Sin. 85, 421–436.
Shen, J., Algeo, T.J., Chen, J., Planavsky, N.J., Feng, Q.L., Yu, J.X., Liu, J.L., 2019b. Mercury in marine Ordovician/Silurian boundary sections of South China is sulfide-hosted and non-volcanic in origin. Earth Planet. Sci. Lett. 511, 130–140.
Shen, J., Yu, J., Chen, J., Algeo, T.J., Xu, G., Feng, Q., Shi, X., Planavsky, N., Shu, W., Xie, S., 2019c. Mercury evidence of intense volcanic effects on land during the Permian-Triassic transition. Geology 47 (12), 1117–1121.
Shen, J., Feng, Q., Algeo, T.J., Liu, J., Zhou, C., Wei, W., Liu, J.S., Them, T.R., Gill, B.C., Chen, J., 2020. Sedimentary host phases of mercury (Hg) and implications for use of Hg as a volcanic proxy. Earth Planet. Sci. Lett. 543, 116333.

Shen, J., Yin, R., Zhang, S., Algeo, T.J., Bottjer, D.J., Yu, J., Xu, G., Penman, D., Wang, Y., Li, L., Shi, X., Planavsky, N.J., Feng, Q., Xie, S., 2022a. Intensified continental chemical weathering and carbon-cycle perturbations linked to volcanism during the Triassic–Jurassic transition. Nat. Commun. 13, 299.
Shen, J., Yin, R., Algeo, T.J., Svensen, H.H., Schoepfer, S.D., 2022b. Mercury evidence for combustion of organic-rich sediments during the end-Triassic crisis. Nat. Commun. 13, 1307.
Shen, J., Chen, J., Yu, J., Algeo, T.J., Smith, R.M.H., Botha, J., Frank, T.D., Fielding, C.R., Ward, P.D., Mather, T.A., 2023. Mercury evidence from southern Pangea terrestrial sections for end-Permian global volcanic effects. Nat. Commun. 14, 6.
Suan, G., Föllmi, K.B., Adatte, T., Bomou, B., Spangenberg, J.E., Van De Schootbrugge, B., 2012. Major environmental change and bonebed genesis prior to the Triassic–Jurassic mass extinction. J. Geol. Soc. Lond. 169 (2), 191–200.
Swift, A., 1999. Stratigraphy (including biostratigraphy). In: Swift, A., Martill, D.M. (Eds.), Fossils of the Rhaetian Penarth Group. The Palaeontological Association, pp. 15–30.
Taylor, S.R., 1983. A stable isotope study of the Mercia Mudstones (Keuper Marl) and associated sulphate horizons in the English Midlands. Sedimentology 30 (1), 11–31.
Taylor, Mclennan, 1985. The Continental Crust: Its Composition and Evolution. Blackwell, Malden, Mass.
Them II, T.R., Jagoe, C.H., Caruthers, A.H., Gill, B.C., Grasby, S.E., Grocke, D.R., Yin, R. S., Owens, J.D., 2019. Terrestrial sources as the primary delivery mechanism of mercury to the oceans across the Toarcian Oceanic Anoxic Event (Early Jurassic). Earth Planet. Sci. Lett. 507, 62–72.
Thibodeau, A.M., Ritterbush, K., Yager, J.A., West, A.J., Ibarra, Y., Bottjer, D.J., Berelson, W.M., Bergquist, B.A., Corsetti, F.A., 2016. Mercury anomalies and the timing of biotic recovery following the end-Triassic mass extinction. Nat. Commun. 7, 11147.
Thomas, J.B., Marshall, J., Mann, A.L., Summons, R.E., Maxwell, J.R., 1993. Dinosteranes (4, 23, 24-trimethylsteranes) and other biological markers in dinoflagellate-rich marine sediments of Rhaetian age. Org. Geochem. 20, 91–104.
Uddin, M.K., 2017. A review on the adsorption of heavy metals by clay minerals, with special focus on the past decade. Chem. Eng. J. 308, 438–462.
Ure, A.M., Davidson, C.M., 2002. Chemical Speciation in the Environment. John Wiley & Sons.
Van Krevelen, D.W., 1981. Coal Science and Technology 3. Coal. Elsevier, Amsterdam, pp. 129–314.
Vejahati, F., Xu, Z., Gupta, R., 2010. Trace elements in coal: associations with coal and minerals and their behavior during coal utilization–a review. Fuel 89 (4), 904–911.
Warrington, G., Cope, J.C.W., Ivimey-Cook, H.C., 2008. Updated proposal for a candidate Global Stratotype Section and Point for the base of the Hettangian Stage, and of the Jurassic System. ISJS Newsletter 35, 2–66.
Warrington, G., Whittaker, A., 1984. The Blue Anchor Formation (late Triassic) in Somerset. Proc. Ussher Soc. 6, 100–107.
Wignall, P.B., 2001. Sedimentology of the Triassic-Jurassic boundary beds in Pinhay Bay (Devon, SW England). Proc. Geol. Assoc. 112 (4), 349–360.
Wignall, P.B., Atkinson, J.W., 2020. A two-phase end-Triassic mass extinction. Earth Sci. Rev. 208, 103282.
Wignall, P.B., Bond, D.P., 2008. The end-Triassic and Early Jurassic mass extinction records in the British Isles. Proc. Geol. Assoc. 119 (1), 73–84.
Wignall, P.B., Bond, D.P., Kuwahara, K., Kakuwa, Y., Newton, R.J., Poulton, S.W., 2010. An 80 million year oceanic redox history from Permian to Jurassic pelagic sediments of the Mino-Tamba terrane, SW Japan, and the origin of four mass extinctions. Glob. Planet. Chang. 71 (1–2), 109–123.
Yager, J.A., West, A.J., Corsetti, F.A., Berelson, W.M., Rollins, N.E., Rosas, S., Bottjer, D. J., 2017. Duration of and decoupling between carbon isotope excursions during the end-Triassic mass extinction and Central Atlantic Magmatic Province emplacement. Earth Planet. Sci. Lett. 473, 227–236.
Yager, J.A., West, A.J., Thibodeau, A.M., Corsetti, F.A., Rigo, M., Berelson, W.M., Bottjer, D.J., Greene, S.E., Ibarra, Y., Jadoul, F., Ritterbush, K.A., Rollins, N., Rosas, S., Di Stefano, P., Sulca, D., Todaro, S., Wynn, P., Zimmermann, L., Bergquist, B.A., 2021. Mercury contents and isotope ratios from diverse depositional environments across the Triassic–Jurassic Boundary: towards a more robust mercury proxy for large igneous province magmatism. Earth Sci. Rev. 223, 103775.
Yamamoto, M., 1996. Stimulation of elemental mercury oxidation in the presence of chloride ion in aquatic environments. Chemosphere 32 (6), 1217–1224.
Yin, R., Feng, X., Chen, B., Zhang, J., Wang, W., Li, X., 2015. Identifying the sources and processes of mercury in subtropical estuarine and ocean sediments using Hg isotopic composition. Environ. Sci. Technol. 49 (3), 1347–1355.
Zhu, Y., La Croix, A., Kemp, D.B., Shen, J., Huang, C., Hua, X., Li, Y., Wei, M., 2024. Are sulfides the primary host of sedimentary Hg? A case study from the lower Jurassic of the Surat Basin (Australia). Chem. Geol. 122028.